12 Impagnatiello F, Guidotti AR, Pesold C, Dwivedi Y, Caruncho H, Pisu MG *et al.* A decrease of reelin expression as a putative vulnerability factor in schizophrenia. *Proc Natl Acad Sci USA* 1998; **95**: 15718–15723.
13 Guidotti A, Auta J, Davis JM, Di-Giorgi-Gerevini V, Dwivedi Y, Grayson DR *et al.* Decrease in reelin and glutamic acid decarboxylase67 (GAD67) expression in schizophrenia and bipolar disorder: a postmortem brain study. *Arch Gen Psychiatry* 2000; **57**: 1061–1069.
14 Eastwood SL, Harrison PJ. Interstitial white matter neurons express less reelin and are abnormally distributed in schizophrenia: towards an integration of molecular and morphologic aspects of the neurodevelopmental hypothesis. *Mol Psychiatry* 2003; **8**: 769, 821–831.
15 Noh JS, Sharma RP, Veldic M, Salvacion AA, Jia X, Chen Y *et al.* DNA methyltransferase 1 regulates reelin mRNA expression in mouse primary cortical cultures. *Proc Natl Acad Sci USA* 2005; **102**: 1749–1754.
16 Ekelund J, Lichtermann D, Hovatta I, Ellonen P, Suvisaari J, Terwilliger JD *et al.* Genome-wide scan for schizophrenia in the Finnish population: evidence for a locus on chromosome 7q22. *Hum Mol Genet* 2000; **9**: 1049–1057.

European Journal of Neuroscience, Vol. 27, pp. 691–701, 2008 doi:10.1111/j.1460-9568.2008.06047.x

Reduction in memory in passive avoidance learning, exploratory behaviour and synaptic plasticity in mice with a spontaneous deletion in the ubiquitin C-terminal hydrolase L1 gene

Mikako Sakurai,[1,*] Masayuki Sekiguchi,[1,2,*] Ko Zushida,[1,2] Kazuyuki Yamada,[3] Satoshi Nagamine,[1] Tomohiro Kabuta[1] and Keiji Wada[1,2]

[1]Department of Degenerative Neurological Diseases, National Institute of Neuroscience, National Center of Neurology and Psychiatry, 4-1-1 Ogawahigashi, Kodaira, Tokyo 187–8502, Japan

[2]CREST, Japan Science and Technology Agency, Kawaguchi, Saitama 322–0012, Japan

[3]Support Unit for Animal Experiments, Brain Science Institute, RIKEN, 2–1 Hirosawa, Wako, Saitama 351–0198, Japan

Keywords: Alzheimer's disease, CREB, hippocampus, LTP, transcription

Abstract

Overexpression of ubiquitin C-terminal hydrolase L1 (UCH-L1) in mice rescues amyloid β-protein-induced decreases in synaptic plasticity and memory. However, the physiological role of UCH-L1 in the brain is not fully understood. In the present study, we investigated the role of UCH-L1 in the brain by utilizing gracile axonal dystrophy (*gad*) mice with a spontaneous deletion in the gene *Uch-l1* as a loss-of-function model. Although *gad* mice exhibit motor paresis beginning at ~ 12 weeks of age, it is possible to analyse their brain phenotypes at a younger age when no motor paresis is evident. Maintenance of memory in a passive avoidance test and exploratory behaviour in an open field test were reduced in 6-week-old *gad* mice. The maintenance of theta-burst stimulation-induced long-term potentiation (LTP) of field synaptic responses from Schaffer collaterals to CA1 pyramidal cells in hippocampal slices was also impaired in *gad* mice. The LTP in *gad* mice was insensitive to actinomycin D, suggesting that a transcription-dependent component of the LTP is impaired. Phosphorylation of cyclic AMP response element binding protein (CREB) in the CA1 region of hippocampal slices from *gad* mice occurred earlier than in the slices from wild-type mice and was transient, suggesting that CREB phosphorylation is altered in *gad* mice. These results suggest that memory in passive avoidance learning, exploratory behaviour and hippocampal CA1 LTP are reduced in *gad* mice. We propose that UCH-L1-mediated maintenance of the temporal integrity and persistence of CREB phosphorylation underlies these impairments.

Introduction

Ubiquitin C-terminal hydrolase L1 (UCH-L1) is a deubiquitinating enzyme (Wilkinson *et al.*, 1989) that is exclusively expressed in the brain and testis, and its expression is neuron-specific in the brain (Wilkinson *et al.*, 1989). Several lines of evidence suggest that UCH-L1 is involved in idiopathic Alzheimer's disease (AD) and Parkinson's disease (PD): (i) UCH-L1 is down-regulated in idiopathic AD and PD (Choi *et al.*, 2004), and in an AD model mouse (Gong *et al.*, 2006); and (ii) UCH-L1 is oxidatively modified in AD brains (Castegna *et al.*, 2002). Substitution of tyrosine for serine at codon 18 (S18Y polymorphism) in the *Uch-l1* gene exerts a protective effect against sporadic AD (Xue & Jia, 2006) and PD (Maraganore *et al.*, 1999). Furthermore, substitution of methionine for isoleucine at codon 93 (I93M mutation) reduces hydrolase activity of UCH-L1 and is linked to a rare autosomal dominant form of familial PD in a German family (Leroy *et al.*, 1998). Although these findings point to a role for UCH-L1 in AD and PD, the physiological role of UCH-L1 in the normal mammalian brain is not fully understood.

UCH-L1 has multiple functions *in vitro*. UCH-L1 removes small adducts or unfolded polypeptides from ubiquitin's C-terminus via hydrolysis (Larsen *et al.*, 1998). In addition, UCH-L1 has ubiquitin-ligase activity on α-synuclein-ubiquitin conjugates (Liu *et al.*, 2002). Apart from enzymatic activity, UCH-L1 acts as a stabilizer of monoubiquitin (Osaka *et al.*, 2003). UCH-L1 is thought to be a therapeutic target for AD; specifically, overexpression of UCH-L1 rescues amyloid β-protein (Aβ)-induced decreases in synaptic plasticity and contextual memory in mice (Gong *et al.*, 2006). Pharmacological suppression of UCH-L1 hydrolase activity (by 70%) is associated with impairment of synaptic transmission, tetanus-induced long-term potentiation (LTP) in the hippocampal CA1 field, and contextual fear memory in mice (Gong *et al.*, 2006). The nonmammalian Aplysia UCH has been identified as an immediate–early gene essential for long-term synaptic facilitation in the nervous system (Hedge *et al.*, 1997).

The aim of the present study was to further characterize the role of UCH-L1 in the mammalian brain. To this end, we utilized the UCH-L1-deficient *gracile axonal dystrophy* (*gad*) mouse, which is a spontaneous mutant with an in-frame deletion in exons 7 and 8 of *Uch-l1* (Saigoh *et al.*, 1999). Expression of the UCH-L1 protein is

Correspondence: Dr Keiji Wada, [1]Department of Degenerative Neurological Diseases, as above.
E-mail: wada@ncnp.go.jp

*M. Sakurai and M. Sekiguchi contributed equally to this study

Received 12 July 2007, revised 10 December 2007, accepted 12 December 2007

undetectable in the central nervous system of *gad* mice (Osaka *et al.*, 2003). In addition, recent analysis in our laboratory suggests that truncated products from the mutant *Uch-l1* are not detected in the *gad* mouse brain (T. Kabuta, unpublished observation). Although *gad* mice exhibit motor paresis beginning at ~12 weeks of age due to axonal degeneration of spinal cord neurons and subsequent degeneration of the spinocerebellar tract (Kikuchi *et al.*, 1990), it is possible to analyse the brain phenotypes of *gad* mice at younger ages when no motor paresis is evident. We found that memory in passive avoidance learning, exploratory behaviour and hippocampal synaptic plasticity are reduced in young *gad* mice (6 weeks of age).

Materials and Methods

Animals

Gad mice were bred at the Experimental Animal Center of the National Institute of Neuroscience, National Center of Neurology and Psychiatry, Tokyo. The original genetic background of *gad* mice was a hybrid of the CBA and RFM strains (Kikuchi *et al.*, 1990). However, *gad* mice were backcrossed to C57BL/6J strain mice 6–18 times before use in the present study. Six-week-old male *gad* mice and wild-type mice generated from heterozygous *gad* mating pairs were used for the experiments. Genotyping was carried out using PCR with the following three primers:

F1, 5′- agcttggagcctgtggtttcaactc-3′;
R1, 5′-tggcagcatcctgaaaaggagaggtg-3′;
R2, 5′-tacagatggccgtccacgttgttga-3′

The reaction conditions were 35 cycles of 94 °C for 20 s, 60 °C for 30 s and 72 °C for 60 s. The wild-type allele produced an 891-bp PCR product, and the *gad* allele produced a 446-bp PCR product. Three to five mice were housed per cage under controlled temperature (25 ± 1 °C) and lighting (12-h light–dark cycle) conditions and provided with food and water *ad libitum*. The experiments were performed in strict accordance with the National Institute of Neuroscience's regulations for animal experimentation, and were approved by the Animal Investigation Committee of the Institute.

Histology

Hematoxylin and eosin (H&E) staining was performed as reported (Kikuchi *et al.*, 1990). For immunohistochemistry, 4-μm-thick paraffin sections were de-paraffinized and pretreated in a microwave oven with 10 mM citrate–NaOH buffer (pH 6.0). After blocking with phosphate-buffered saline containing 1% heat-inactivated normal goat serum and 0.1% [(v/v)] Triton X-100, slides were incubated with an anti-Aβ monoclonal antibody (clone 4G8, 1 : 100 dilution; Signet Laboratories, Dedham, MA, USA) or an antisynaptophysin monoclonal antibody (MAB5258, 1 : 500 dilution; Chemicon, Temecula, CA, USA) and then with Envision+horseradish peroxidase–labelled anti-mouse IgG (DakoCytomation Inc., Carpinteria, CA, USA). Chromogenic detection was performed using the DAB Substrate kit (DakoCytomation Inc.). Sections were examined with a BX51 microscope (Olympus).

Behavioural tests

One-trial passive avoidance tests were performed as described (Yamada *et al.*, 2003). Briefly, a single mouse was introduced into a light compartment of a light–dark box (Muromachi-kikai, Tokyo, Japan). During habituation, mice were allowed to freely explore the box for 5 min with the sliding door between the light and dark compartments open; after that, the mice were returned to their home cage. For conditioning, which was carried out 2 h after habituation, the mice were introduced into the light compartment, the sliding door was closed when both hindlimbs had entered into the dark box, and an electrical footshock was delivered via the floor grid in the dark compartment (300 μA, 3 s duration, using a shock generator–scrambler; Muromachi-kikai). The mice were left in the light–dark box for 5 min and then returned to their home cage. Tests were carried out 2 or 24 h after the conditioning by re-introducing the mice into the light compartment of the light–dark box. The latency time for mice to enter the dark compartment was measured (light–dark latency, with a 5 min cut-off). The tests at 2 and 24 h postconditioning were carried out using different groups of mice.

The pain sensitivity of mice was tested as described (Yamada *et al.*, 2003). Briefly, a series of footshocks of ascending (20, 40, 60, 80, 100 and 130 μA, 1 s duration) and descending (130, 100, 80, 60, 40 and 20 μA, 1 s duration) current were serially delivered to the mice via the floor grid. The input current that induced hindlimb withdraw was recorded. The interfootshock interval was 15 s. This trial was performed six times, and the data were averaged.

Open field tests were performed as we described (Zushida *et al.*, 2007). Briefly, the test was carried out in an arena (a 50 × 50 cm white field surrounded by a 40-cm-high white wall, illuminated with 80 lx) placed in a soundproof box. Mice were placed at the periphery of the arena, and for 5 min the behaviour of the mice was recorded using a digital video camera linked to a computer. Locomotor activity was calculated from this record by Image OF (O'Hara & Co., Ltd, Tokyo, Japan), modified software based on the public domain NIH Image program. Rearing was manually counted.

The light–dark box test was performed as described (Yamada *et al.*, 2002). Briefly, mice were placed into the dark compartment of the light–dark box and were allowed to explore both sides of the light–dark box for 5 min. During these 5 min, three parameters were measured: latency to enter the light compartment, number of entries into the light compartment, and duration in the light compartment.

Electrophysiology

Each 6-week-old male mouse was anaesthetized with halothane, and the brain was quickly removed. Preparation of hippocampal slices for electrophysiology was carried out as reported (Takamatsu *et al.*, 2005; Zushida *et al.*, 2007). Briefly, the hippocampus was isolated from the brain, and transverse slices (400 μm thick) were prepared using a Vibratome 3000 microtome (Vibratome Company, St Louis, MO, USA) in a sucrose-based cutting solution (in mM: sucrose, 234; KCl, 25; NaH_2PO_4, 1.25; $MgSO_4$, 10; $NaHCO_3$, 26; glucose, 11; and $CaCl_2$, 0.5). The slices were maintained at room temperature in artificial cerebrospinal fluid (ACSF; in mM: NaCl, 125; KCl, 4.4; $MgSO_4$, 1.5; NaH_2PO_4, 1.0; $NaHCO_3$, 26; glucose, 10; and $CaCl_2$, 2.5; pH 7.4, 290–300 mOsm/L) continuously bubbled with 95% O_2 and 5% CO_2. A slice was then transferred to the recording chamber and was continuously superfused at 3 mL/min with ACSF maintained at 28–32 °C.

Extracellular field recordings were carried out as reported (Takamatsu *et al.*, 2005). Briefly, field excitatory postsynaptic potentials (fEPSPs) were recorded from CA1 stratum radiatum of the hippocampus using a glass micropipette (1–2 MΩ) filled with ACSF. The electrical signals were amplified using a MultiClamp 700B amplifier (Axon Instruments, Foster City, CA, USA), filtered at 10 kHz, digitized at 10 kHz and acquired with Clampex (ver. 9.2). A bipolar stainless steel stimulating electrode was placed in stratum radiatum at the border between CA2 and CA3 to stimulate the Schaffer collateral pathway. The pulse intensity was adjusted to give 40% of the maximum amplitude in all experiments. Stimulation was carried out in

constant current mode (100 μs duration). The fEPSPs for which the 40% amplitude was > 1 mV were used for data analysis. The strength of synaptic transmission was determined by measuring the rising phase (20–60%) of the fEPSP slope. The average fEPSP slope during the 10 min prior to LTP induction was taken as the baseline, and all values were normalized to this baseline. The baseline stimulation frequency was 0.033 Hz. LTP was induced by applying theta-burst stimulation (TBS; 15 bursts of four pulses at 100 Hz, delivered at an interburst interval of 200 ms) or tetanic stimulation (100 Hz, 1 s, three times with a 20 s interval). Paired-pulse facilitation was induced by delivering two consecutive pulses with a 20-, 50-, 100-, 200- or 400-ms interpulse interval.

Somatic whole-cell patch-clamp recordings were made with a MultiClamp 700B amplifier (Zushida *et al.*, 2007). Pyramidal-shaped neurons in the CA1 pyramidal layer visually identified with differential contrast video microscopy (Hamamatsu Photonics, Hamamatsu, Japan) on an upright microscope (Axioscope, Zeiss, Oberkochen, Germany) were selected for recording. The patch electrodes were 6–10 MΩ when filled with a solution containing (in mM): K gluconate, 132; KCl, 3; HEPES, 10; EGTA, 0.5; $MgCl_2$, 1; sodium phosphocreatine, 12; ATP·Mg, 3; and GTP, 0.5 (pH 7.4 with KOH, 285–290 mOsm/L). We used this solution when measuring membrane potential and input resistance. The input resistance was calculated by injecting a square current pulse (−10 pA) in current-clamp mode. For comparison of synaptic currents at −70 and +40 mV, an internal solution containing (in mM): CsOH, 105; CsCl, 30; HEPES, 10; EGTA, 0.5; $MgCl_2$, 1; sodium phosphocreatine, 12; ATP·Mg, 3; and GTP, 0.5 (pH 7.3 with gluconic acid, 295 mOsm/L) was used. The signal was digitized at one point per 50 μs and stored using Clampex. The resting membrane potential of the cells used in the analysis ranged from −57 to −67 mV, and the series resistance was 3–20 MΩ. Synaptic responses were elicited by electrical stimulation as described for extracellular recording. The pulse intensity was adjusted to elicit excitatory postsynaptic potentials (EPSPs) 40% of the amplitude required for action potential generation in current-clamp mode.

All chemicals and drugs used for electrophysiology were purchased from Sigma with the exception of actinomycin D, which was obtained from Wako Pure Chemicals (Tokyo, Japan). Actinomycin D was dissolved in dimethylsulfoxide at 40 mM, added to ACSF just prior to application at 40 μM, and bath-applied with perfusion. Therefore, the final dimethylsulfoxide concentration was 0.1%.

Western blotting

For analysis of Aβ, the hippocampus was isolated from the brain and snap-frozen in liquid nitrogen. The tissue was homogenized in ice-cold buffer (Tris-HCl, 50 mM; NaCl, 150 mM; EDTA, 5 mM; and Triton X-100, 1%; pH 7.5) containing proteinase inhibitors (Complete, EDTA-free; Roche Applied Science, Indianapolis, IN, USA) and phosphatase inhibitors (Halt phosphatase inhibitor cocktail; Pierce, Rockford, IL, USA), and the homogenate was subjected to SDS-PAGE. Western blotting was carried out as we reported (Kabuta *et al.*, 2006) using anti-Aβ (clone 4G8; Signet Laboratories), anti-UCH-L1 (UltraClone Ltd, UK) and anti-β-actin (Sigma) antibodies. Briefly, immunoreactive signals were visualized with SuperSignal West Femto maximum sensitivity substrate (Pierce) or SuperSignal West Dura extended duration substrate (Pierce) and detected with a chemiluminescence imaging system (FluorChem; Alpha Innotech, San Leandro, CA, USA). Human Aβ 1–42 from Peptide Institute, Inc., Osaka, Japan served as the positive control.

Following extracellular recording, hippocampal slices were retrieved for Western blotting. The dentate gyrus and CA3 region of the slices were cut off, and the remaining CA1 region was snap-frozen in liquid nitrogen. Tissue samples from each slice were homogenized in the same buffer as used for the Aβ analysis, and the homogenate was subjected to SDS-PAGE. The antibodies used were anti-phospho-CREB (serine 133), anti-CREB (Cell Signalling Technology, Inc., Danvers, MA, USA), anti-cAMP-dependent protein kinase (protein kinase A; PKA) regulatory subunit RIα and RIIα (BD Biosciences, San Jose, CA, USA), anti-UCH-L1 (UltraClone Ltd) and anti-β-actin (Sigma). Immunoreactive signals were visualized as described for the Aβ analysis. The signal intensity was quantified by densitometry using FluoChem software (Alpha Innotech).

Data and statistical analysis

Numerical data are expressed as the mean ± SEM. The two-tailed Student's *t*-test was used for comparison between wild-type mice and *gad* mice. Repeated-measures one-way ANOVA was used to analyse whether footshock and exposure to an open field arena had significant effects within a genotype in passive avoidance and open field tests, respectively. ANOVA with the Bonferroni–Dunn test was used to compare the three data groups in the pCREB analysis.

Results

Structural abnormalities were not detected in the cerebrum and hippocampus of young gad mice

Before behavioural analysis, we first examined whether there were any histological abnormalities in the cerebral cortex and hippocampus of 6-week-old *gad* mice. It has been reported that the thalamus is not impaired in *gad* mice (Kikuchi *et al.*, 1990), but there is no report on the cortex and limbic system. Figure 1A–D shows H&E staining of coronal brain sections (at bregma level −1.7 mm) from a wild-type mouse (Fig. 1A and C) and *gad* mouse (Fig. 1B and D; 6 weeks of age). We could not detect any visible abnormalities, such as atrophy or lack of cells, in the hippocampus or cortex of *gad* mice ($n = 2$). One anatomical characteristic of *gad* mice is spheroid structures in the medulla and spinal cord that are thought to be degenerating axons (Kikuchi *et al.*, 1990). We did not find this aberration in the hippocampus or cortex of *gad* mice (Fig. 1A–D). We also examined other brain regions in sections cut at bregma levels 2.5, 1.0, −3.0 and −6.0 mm, and no outstanding abnormalities were evident in the *gad* mice (data not shown). In addition, we carried out immunohistochemical staining using antisynaptophysin. This antibody stains presynaptic sites and thus the staining pattern would be expected to be different in *gad* mice if there was noticeable axonal degeneration. Typical punctate synaptophysin staining was obtained in both wild-type (Fig. 1E and G) and *gad* (Fig. 1F and H) mice. We could not detect any visible differences in the staining of the hippocampus between wild-type and *gad* mice. These results suggest that structural impairment of the brain at a macroanatomical level is not evident in 6-week-old *gad* mice.

Axonal degeneration promotes accumulation of Aβ in the medulla and spinal cord of *gad* mice (Ichihara *et al.*, 1995). Consistent with the lack of spheroid structures in the cortex and hippocampus, we did not find abnormal accumulation of Aβ in these brain regions in *gad* mice up to 12 weeks of age (immunohistochemical analysis using an antibody to Aβ; data not shown). Furthermore, we examined nonfibrillar Aβ by Western blotting. We could not detect any significant bands in the samples from wild-type and *gad* mouse hippocampi when blotting with anti-Aβ (Fig. 1I, upper panel). Authentic human Aβ (the right two lanes, a positive control) blotted

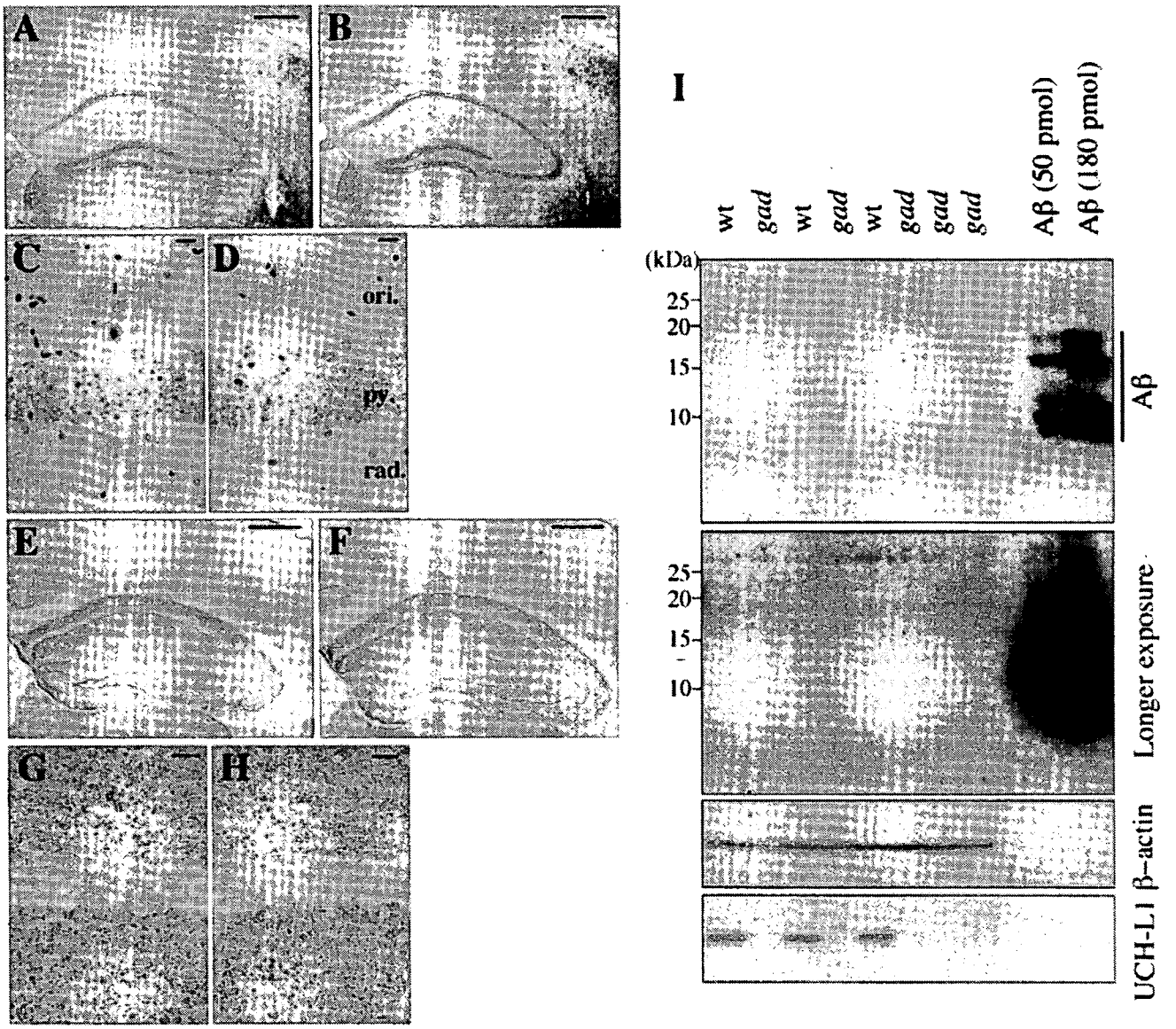

FIG. 1. Six-week-old *gad* mice have normal brain histology. (A–D) H&E staining of coronal brain sections from (A and C) a 6-week-old wild-type (wt) mouse and (B and D) a 6-week-old *gad* mouse. (C and D) A higher magnification of the hippocampal CA1 field. ori., stratum oriens; py., pyramidal cell layer; rad., stratum radiatum. (E–H) Synaptophysin immunohistochemistry in coronal brain sections from a six-week-old wt mouse (E and G) and a six-week-old *gad* mouse (F and H). (G and H) A higher magnification of the hippocampal CA1 field. (I) Western blotting of samples prepared from the hippocampi of three wt and five *gad* mice. Antibodies against Aβ, β-actin and UCH-L1 were used. Authentic Aβ was used as a positive control. A short exposure is shown in the upper panel; a longer exposure is shown below. Molecular size markers (kDa) are shown on the left. Scale bars, 500 μm (A, B, E and F), 20 μm (C, D, G and H).

densely on the same membrane. After a longer exposure (Fig. 1I) we could detect certain bands, but there was no band that was significantly increased in *gad* mice compared with wild-type mice. Blots using antiβ-actin and anti-UCH-L1 were carried out to confirm the sample load and genotype, respectively (Fig. 1I).

Lack of UCH-L1 in mice impaired memory maintenance in the passive avoidance test and exploratory behaviour for a novel environment

Next, we examined whether lack of UCH-L1 had a detectable impact on mouse behaviour. For this purpose, we carried out one-trial passive avoidance tests. Figure 2A shows the performance of wild-type and *gad* mice in this test. After habituation to the light–dark box, mice were conditioned with an electrical footshock when they entered the dark compartment. We then tested their ability to avoid the dark compartment 24 h after the conditioning footshock. The footshock significantly prolonged the light–dark latency in wild-type mice (comparison of the conditioning and test sessions $P = 0.003$, $F = 14.6$, $n = 12$; repeated-measures ANOVA). In contrast, the light–dark latency was not significantly affected in *gad* mice (comparison of the conditioning and test sessions using repeated-measures ANOVA, $P = 0.2437$, $F = 1.556$, $n = 10$), suggesting that memory function, as assessed by this test, is impaired in *gad* mice. In

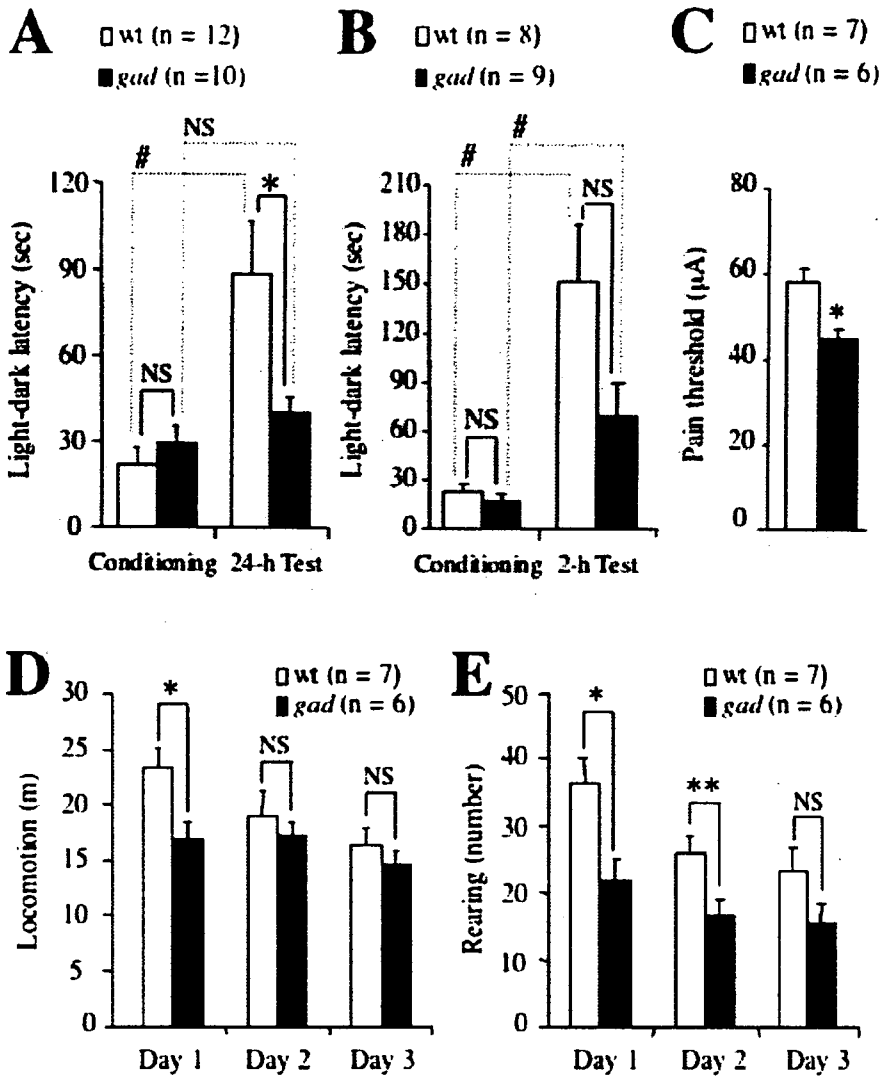

FIG. 2. Impairment of memory maintenance and exploratory behaviour in *gad* mice. (A and B) Light–dark latency of mice in a one-trial passive avoidance test. After habituation to a light–dark box, mice were conditioned with an electrical footshock when they entered the dark compartment (Conditioning). At (A) 24 h or (B) 2 h after the footshock, the mice were reintroduced into the light–dark box and the time for mice to enter the dark compartment (light–dark latency) was measured (Test). $^{*}P = 0.028$; NS, not significant; two-tailed Student's *t*-test (solid lines). $^{\#}P < 0.020$; NS, not significant, repeated-measures one-way ANOVA (dotted lines). (C) Pain sensitivity of the mice was measured by applying a series of electrical footshocks. $^{*}P = 0.002$, two-tailed Student's *t*-test. (D) Locomotor activity of wild-type and *gad* mice in an open field arena. The mice were introduced into the arena for the first time on day 1. $^{*}P = 0.023$, two-tailed Student's *t*-test. (E) Rearing frequency of wild-type and *gad* mice in an open field arena. $^{*}P = 0.014$, $^{**}P = 0.021$; two-tailed Student's *t*-test.

addition, the light–dark latency in the 24-h test session differed significantly between the wild-type and *gad* mice ($P = 0.028$; two-tailed Student's *t*-test). We next conducted a test session 2 h after conditioning to test whether learning ability was impaired in *gad* mice shortly after conditioning. In the test 2 h after conditioning (Fig. 2B), the footshock had a significant effect on the light–dark latency in both wild-type and *gad* mice ($P = 0.0147$, $F = 10.356$, $n = 8$ for wild-type mice; $P = 0.0199$, $F = 8.407$, $n = 9$ for *gad* mice; repeated-measures ANOVA). The average latency in the 2-h test session did not differ significantly between the wild-type and *gad* mice ($P = 0.074$; two-tailed Student's *t*-test). These results suggest that *gad* mice are able to learn but maintenance of memory is reduced. Because the pain sensitivity of *gad* mice was greater than that of wild-type mice (Fig. 2C; $P = 0.002$ with two-tailed Student's *t*-test), the footshock used for conditioning was indeed an aversive stimulus in *gad* mice.

Next, we carried out the open field test. Mice were exposed to an open field arena for the first time on day 1 (Fig. 2D). The wild-type mice explored the novel environment and showed high locomotor activity (Fig. 2D). Locomotor activity was reduced upon re-exposure of wild-type mice to the same arena on days 2 and 3 because they remembered the arena, and thus the novelty was reduced ($P = 0.024$, $F = 12.928$, $n = 7$; repeated-measures ANOVA). In contrast, locomotor activity was not significantly decreased in *gad* mice ($P = 0.392$, $F = 1.030$, $n = 6$; repeated-measures ANOVA). The locomotor activity on day 1 differed significantly between wild-type and *gad* mice ($P = 0.023$; two-tailed Student's *t*-test), but the activity on day 2 or 3 did not ($P = 0.500$ and 0.446 for days 2 and

3, respectively). To determine whether the difference in locomotor activity on day 1 was due to reduced exploratory behaviour in *gad* mice, we measured the frequency of rearing, a typical exploratory behaviour (Lever *et al.*, 2006; Fig. 2E). Similar to locomotor activity, upon re-exposure rearing frequency decreased in wild-type mice ($P = 0.009$, $F = 14.257$, $n = 7$; repeated-measures ANOVA) but not in *gad* mice ($P = 0.131$, $F = 2.503$, $n = 6$; repeated-measures ANOVA). The rearing frequency on days 1 and 2 differed significantly between wild-type and *gad* mice ($P = 0.014$ and 0.021 for days 1 and 2, respectively; two-tailed Student's *t*-test), but the activity on day 3 did not ($P = 0.093$). These results suggest that exploratory behaviour in a novel environment is reduced in *gad* mice.

Although these data apparently suggest that memory in passive avoidance learning and exploratory behaviour are reduced in young *gad* mice, there is a possibility that the anxiety state of *gad* mice is altered. Alterations in the anxiety state can affect memory (Bouton *et al.*, 1990) and the response to novel environments. To measure anxiety, we performed a light–dark box test. In this test, mice usually avoid the light compartment. Therefore, the level of anxiety can be measured as the latency to move into the light compartment and the duration of time in the light compartment (Yamada *et al.*, 2002). Because the passive avoidance test also utilizes these properties, performance in the light–dark test is important for interpreting the results from the passive avoidance test. The time required for the mice to step into the light compartment when introduced into the dark compartment (dark-light latency; Fig. 3A), the time the mice spent in the light compartment (Fig. 3A) and the number of times the mice crossed between compartments (Fig. 3B) did not differ significantly between wild-type and *gad* mice ($P = 0.834$, 0.417 and 0.109, respectively; two-tailed Student's *t*-test). These results suggest that anxiety state, as assessed by this test, was not obviously altered in *gad* mice. Therefore we concluded that the impairments in passive avoidance learning and exploratory behaviour were not due to alterations in the anxiety state.

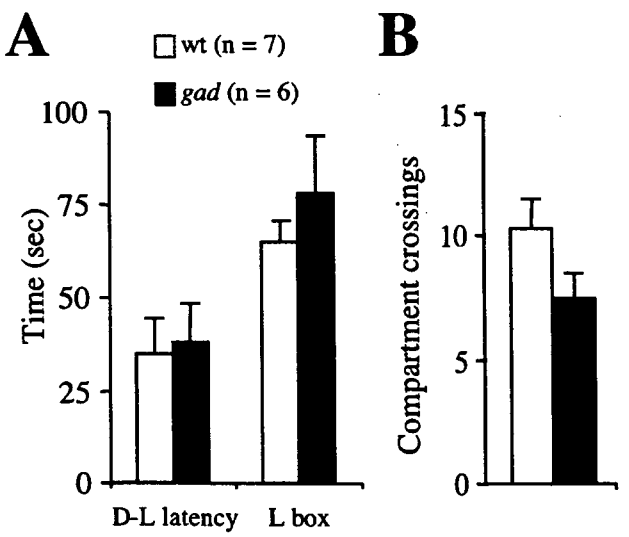

FIG. 3. Wild-type and *gad* mice performed similarly in the light–dark box test. (A) Dark–light (D-L) latency and duration of time in the light compartment (L box). (B) Number of crossings between the two compartments.

Impairment of a transcription-dependent component of LTP in gad mice

We tested whether the lack of UCH-L1 affects neuronal function by measuring LTP at Schaffer collateral synapses onto CA1 pyramidal neurons in hippocampal slice preparations. LTP is believed to be a synaptic mechanism underlying memory and learning (Bliss & Collingridge, 1993). The CA1 synapse was selected because this brain region is involved in spatial memory (Morris *et al.*, 1982) and passive avoidance memory (Bevilaqua *et al.*, 1997; Impey *et al.*, 1998). In wild-type slices, TBS induced robust LTP at CA1 synapses (Fig. 4A), as reported for C57BL/6J mice (Nguyen & Kandel, 1997; Nguyen *et al.*, 2000). In contrast, TBS-induced LTP was attenuated in *gad* mice beginning ~20 min post-TBS (Fig. 4A). At 45 min post-TBS, normalized synaptic responses were significantly greater in wild-type slices (1.87 ± 0.08, $n = 7$) than in *gad* slices (1.36 ± 0.07, $n = 6$; $P = 0.001$, two-tailed Student's *t*-test). Impairment of LTP in *gad* mice depended on the stimulation pattern. Tetanus-induced LTP was identical in wild-type and *gad* mice (Fig. 4B; normalized fEPSP slopes at 45 min post-tetanus: wild-type, 1.81 ± 0.16, $n = 5$; *gad*, 1.86 ± 0.25, $n = 5$).

Stimulus–output curves (Fig. 5A) and paired-pulse facilitation (Fig. 5B) of CA1 synapses were essentially identical in wild-type and *gad* mice. The latter result suggests that a postsynaptic, rather than presynaptic, mechanism is involved in impairment of TBS-induced LTP in *gad* mice. LTP at this synapse is dependent on postsynaptic NMDA receptors (Harris *et al.*, 1984; Larson & Lynch, 1988). Therefore, we tested whether NMDA receptor activity was reduced in *gad* mice using patch-clamp recordings. For this purpose, we recorded Schaffer collateral–CA1 synaptic responses in neurons voltage-clamped to −70 and +40 mV in the presence of picrotoxin (50 μM). The amplitude of the synaptic response recorded at +40 mV at 100 ms poststimulation was normalized to the peak amplitude of the response at −70 mV to estimate the ratio of NMDA-mediated to non-NMDA-mediated currents (Fig. 5D). Because superfusion of the slices with picrotoxin frequently elicited epileptiform activity (data not shown), three to five synaptic responses without epileptiform activity were selected and averaged. The ratio was identical in wild-type and *gad* mice (0.45 ± 0.05, $n = 5$ and 0.43 ± 0.05, $n = 7$ for wild-type and *gad* mice, respectively; two-tailed Student's *t*-test). Therefore, attenuation of synaptic NMDA receptor activity does not account for reduced LTP in *gad* mice. Resting membrane potential and input resistance of CA1 pyramidal neurons did not differ substantially between wild-type and *gad* mice [resting membrane potential, -60.1 ± 0.4 mV for wild-type mice ($n = 20$) and -60.0 ± 0.6 mV for *gad* mice ($n = 20$); input resistance, 163 ± 9.6 for wild-type mice ($n = 16$) and 175 ± 10.8 for *gad* mice ($n = 13$); results obtained from the records using potassium-gluconate pipette solution].

CA1 LTP is composed of early and late temporal phases (Nguyen *et al.*, 1994; Abel *et al.*, 1997; Nguyen & Kandel, 1997). The former is induced mainly by an increase in the number of AMPA-type glutamate receptors at the synapse (reviewed in Malinow & Malenka, 2002) whereas the latter is induced by new protein synthesis from transcription of new mRNA (Nguyen *et al.*, 1994) and/or local protein synthesis from previously expressed mRNA (Bradshaw *et al.*, 2003). Because no obvious changes in the early phase of LTP (up to ~20 min post-TBS) were observed in *gad* mice, we tested whether the late phase is occluded in *gad* mice. For this purpose, we applied actinomycin D, a transcription inhibitor, to the slices and compared suppression of TBS-induced LTP in wild-type and *gad* mice. In wild-type mice, the maintenance of TBS-induced LTP was suppressed by actinomycin D (Fig. 6A). The normalized fEPSP slope at 45 min

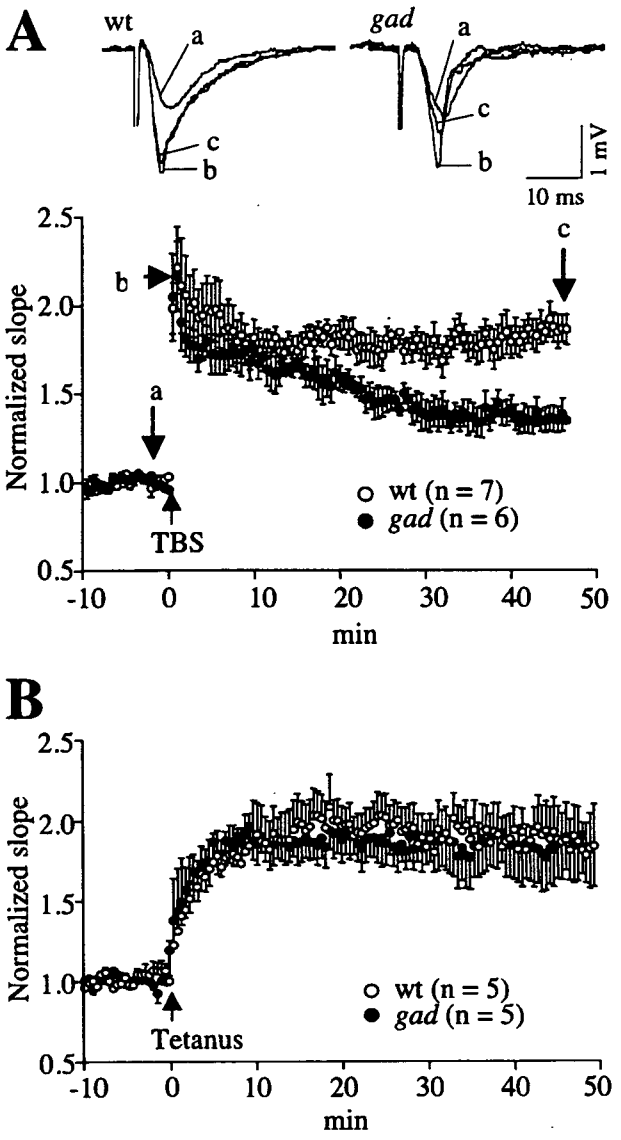

FIG. 4. TBS-induced LTP in area CA1 of the *gad* mouse hippocampus was impaired. (A) LTP induced by TBS in wild-type (○) and *gad* (●) mice. The fEPSP slope was normalized to baseline (pre-TBS) values. Typical fEPSP traces are shown above. Traces were recorded (a) just before TBS, (b) immediately after TBS and (c) 45 min after TBS. (B) Tetanus-induced LTP was identical in wild-type and *gad* mice.

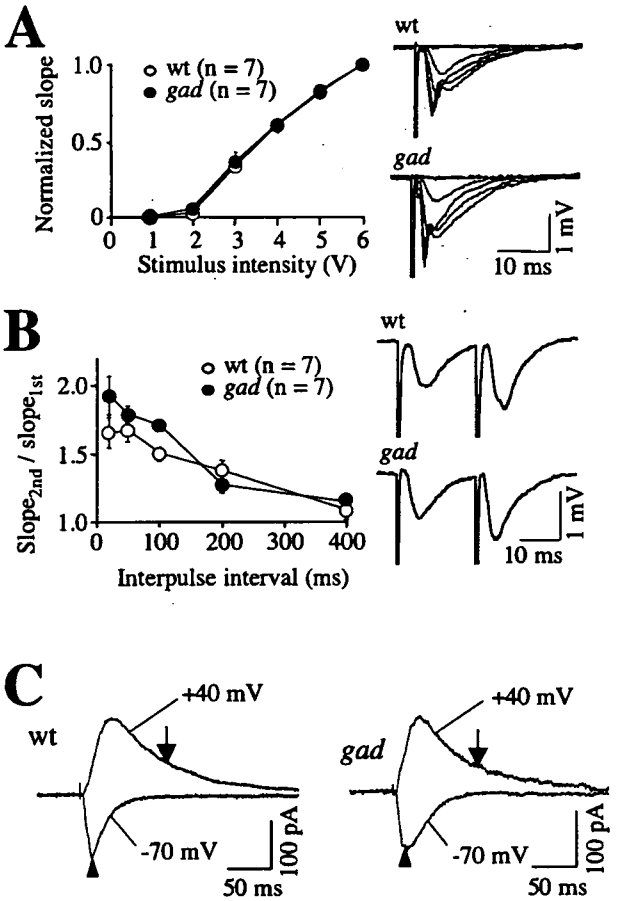

FIG. 5. Stimulus–output curves, paired-pulse facilitation and NMDA receptor-mediated currents were similar in wild-type and *gad* mice. (A) The relation between stimulus intensity and the slope of the fEPSP was identical in wild-type and *gad* mice. For each slice, fEPSP slopes elicited by six different stimulus intensities (1–6 V; sample traces in the right panel) were normalized to the value obtained using 6-V stimulation, and then normalized values were averaged. (B) Paired-pulse facilitation of fEPSPs did not differ substantially between wild-type and *gad* mice. (C) The ratio of NMDA receptor-mediated currents to non-NMDA receptor-mediated currents was identical in wild-type and *gad* mice. Patch-clamp recordings from neurons voltage-clamped to −70 and +40 mV. The arrowhead indicates the peak of the non-NMDA receptor-mediated current, and the arrow indicates 100 ms poststimulation for the NMDA receptor-mediated current; current amplitudes at these points were used for the ratio.

post-TBS was 1.43 ± 0.07 (n = 5) in the presence of actinomycin D, and this value differed significantly from that in wild-type hippocampal slices without actinomycin D (1.87 ± 0.08, P = 0.003; two-tailed Student's t-test). This result agrees with a previous report (Nguyen & Kandel, 1997). In contrast, TBS-induced LTP in *gad* mice was insensitive to actinomycin D (Fig. 6B). The normalized fEPSP slope at 45 min post-TBS was 1.36 ± 0.04 (n = 5) in the presence of actinomycin D and did not differ significantly from the value in *gad* hippocampal slices without actinomycin D (1.36 ± 0.07, P = 0.948; two-tailed Student's t-test). These results suggest that a transcription-dependent component of LTP is impaired in *gad* mice. In both wild-type and *gad* mice, actinomycin D did not affect the baseline fEPSP slope (without TBS) up to 80 min postapplication (Fig. 6C and D).

CREB phosphorylation was altered in gad mice

Late-phase LTP in the hippocampal CA1 field requires transcription elicited by phosphorylation of serine 133 on cAMP response element binding protein (CREB; Nguyen *et al.*, 1994). In addition, Aplysia UCH is involved in persistent activation of PKA during long-term synaptic facilitation (Hedge *et al.*, 1997). From these reports and our experiments using actinomycin D above, we suspected that phosphorylated CREB (pCREB)-induced transcription is disrupted in *gad* mice. To address this, we analysed pCREB in the CA1 field of slices used

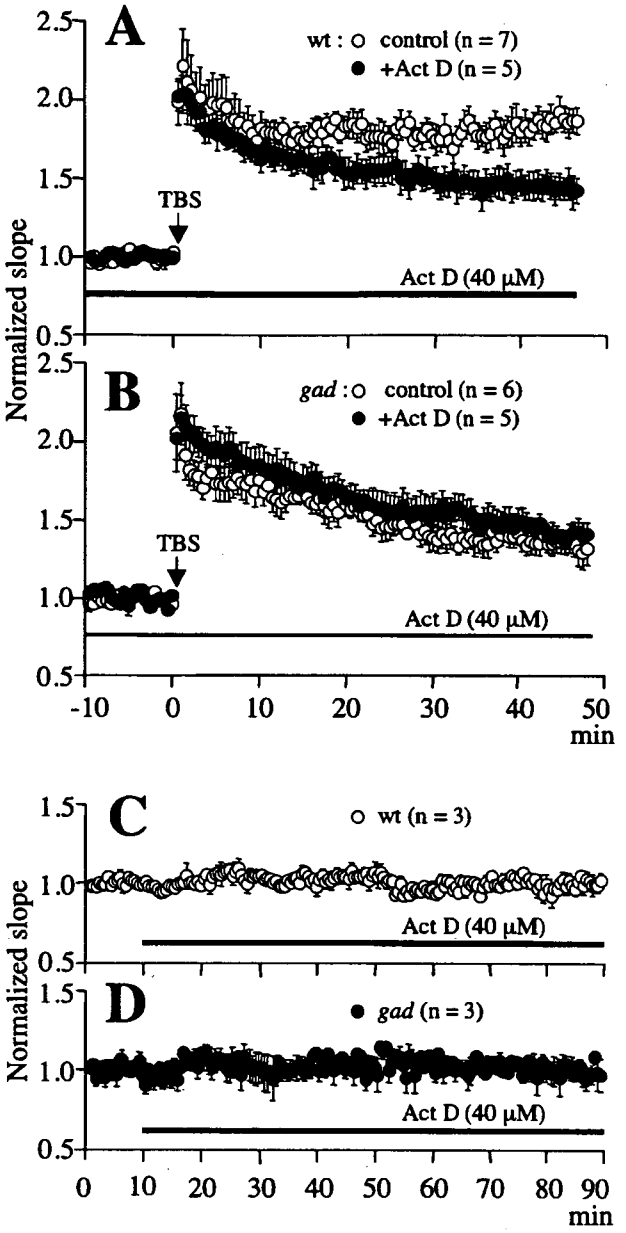

FIG. 6. Transcription-dependent LTP was impaired in *gad* mice. (A and B) Actinomycin D (Act D) suppressed late-phase LTP in (A) wild-type mice but (B) had no effect in *gad* mice. Act D was applied 10 min before LTP induction and was continuously applied until 50 min post-TBS. LTP in the absence of Act D (control) has been reproduced from Fig. 4. (C and D) Without TBS, Act D had no effect on the normalized fEPSP slope in either (C) wild-type or (D) *gad* mice.

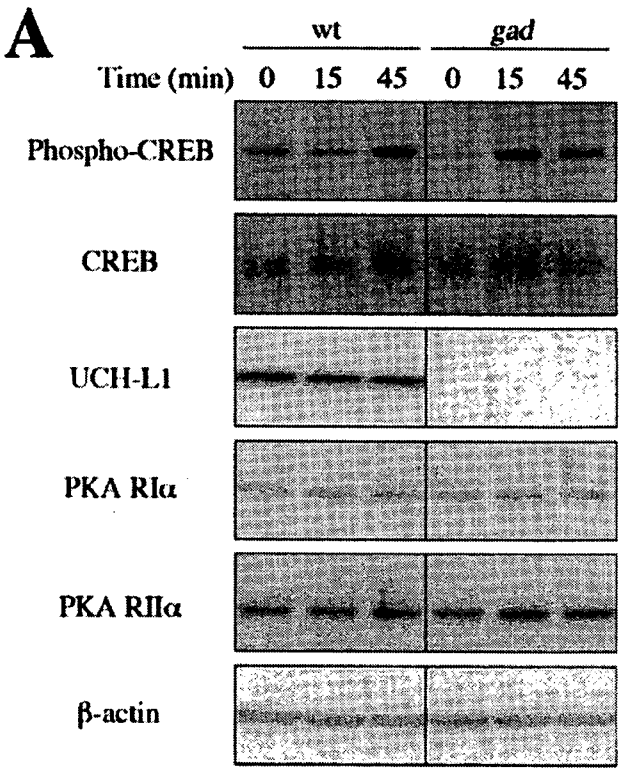

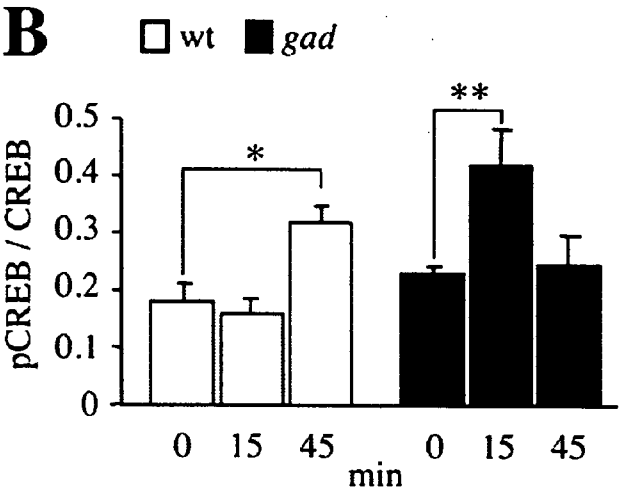

FIG. 7. CREB phosphorylation was altered in *gad* mice. (A) Western blotting of samples prepared from hippocampal slices recovered pre-TBS (0), 15 min post-TBS (15) or 45 min post-TBS (45). Primary antibodies are indicated to the left of the blots. Similar results were obtained at each time point in six slices from wild-type mice and five slices from *gad* mice. (B) The normalized band density of pCREB to CREB at time 0 (pre-TBS), 15 min and 45 min post-TBS in wild-type ($n = 5$) and *gad* ($n = 4$) mice. *$P = 0.012$ and **$P = 0.014$, Bonferroni–Dunn test.

for electrophysiological recording by Western blotting (Fig. 7A). In wild-type mice, pCREB levels at 15 min post-TBS did not differ from pre-TBS levels, but at 45 min post-TBS levels were increased relative to pre-TBS levels. The onset of CREB phosphorylation (45 min postconditioning) is in agreement with a previous report (Ahmed & Frey, 2005). In *gad* mice, however, pCREB levels were increased at 15 min post-TBS but not maintained at 45 min post-TBS (Fig. 7A). Unphosphorylated CREB levels were similar among samples (Fig. 7A). Similar results were obtained in slices from five wild-type and four *gad* mice. In each set of slices, the band density of pCREB was normalized to that of CREB and the values were averaged (Fig. 7B). In wild-type mice (Fig. 7B), the normalized pCREB levels at 15 min post-TBS did not differ significantly from pre-TBS levels

($P = 0.656$; Bonferroni–Dunn test) but at 45 min post-TBS pCREB levels were significantly higher than pre-TBS levels ($P = 0.012$). In *gad* mice (Fig. 7B), pCREB levels were significantly higher at 15 min post-TBS ($P = 0.014$), but at 45 min post-TBS pCREB levels were not significantly different from pre-TBS levels ($P = 0.393$). These results suggest that the onset and persistence of CREB phosphorylation are altered in *gad* mice.

In Aplysia, serotonin stimulation that induces synaptic plasticity increases expression of UCH by about five-fold. The increased UCH expression stimulates proteasomal degradation of the PKA regulatory subunit N4, thereby inducing persistent PKA activity (Hedge *et al.*, 1997). To determine whether this process also exists in mice, we analysed UCH-L1 and PKA regulatory subunits Iα and IIα in the CA1 field of hippocampal slices by Western blotting. As Fig. 7A shows, the level of UCH-L1 was not obviously affected by TBS at either 15 or 45 min post-TBS in wild-type mice. For quantitative analysis, the band density of UCH-L1 was normalized to that of β-actin and the normalized value was then further normalized to pre-TBS values. At 15 and 45 min post-TBS, the normalized values were 1.00 ± 0.24 ($n = 5$) and 1.06 ± 0.21 ($n = 5$), respectively, confirming that UCH-L1 levels were unchanged. Similarly, TBS-induced changes in the levels of PKA regulatory subunit Iα and IIα were also not apparent in either type of mouse (Fig. 7A). For example, the relative band-density of PKA IIα normalized to β-actin was 1.03 ± 0.14 (15 min post-TBS) and 1.06 ± 0.12 (45 min post-TBS) for wild-type mice ($n = 5$). In *gad* mice ($n = 4$), values were 1.02 ± 0.20 (15 min post-TBS) and 1.01 ± 0.25 (45 min post-TBS). For pre-TBS, the relative band-density of PKA IIα normalized to β-actin also did not differ between wild-type and *gad* mice [the normalized value for *gad* mice/the normalized value for wild-type mice was 0.96 ± 0.10 ($n = 4$)].

Discussion

In this study, we demonstrated that UCH-L1 is required for (i) maintenance of memory in a passive avoidance test and exploratory behaviour in a novel environment, and (ii) a transcription-dependent component of TBS-induced LTP in area CA1 of the hippocampus. UCH-L1 may be essential in transcription-dependent TBS-LTP because it maintains the integrity of TBS-induced CREB phosphorylation. No outstanding forebrain atrophy or aberrant structures were evident in 6-week-old *gad* mice at the level of the light microscope. Thus, the functional abnormalities caused by the lack of UCH-L1 occurred in the absence of any detectable gross structural abnormalities in the brain. However, abnormalities in neuron morphology, such as spine morphology or density, remain a possibility in *gad* mice.

Several studies suggest that synaptic and memory abnormalities precede neuronal cell death in AD (Yao *et al.*, 2003) and in AD model mice (Chapman *et al.*, 1999; Freir *et al.*, 2001; Snyder *et al.*, 2005; Shemer *et al.*, 2006), which supports the hypothesis that synapses may be an initial target in AD (Small *et al.*, 2001; Selkoe, 2002). Aβ is thought to be one of the major players that disrupt synaptic function (reviewed in Selkoe, 2002). Because we have shown here that UCH-L1 is essential for memory maintenance, exploratory behaviour and a particular form of hippocampal LTP, it is possible that the AD-associated reduction in UCH-L1 (Choi *et al.*, 2004) further exacerbates the synaptic and memory deficits induced by Aβ accumulation. In addition, glutamate-induced CREB phosphorylation is decreased by Aβ treatment of cultured hippocampal neurons (Vitolo *et al.*, 2002). Thus, accumulation of Aβ and reduction of UCH-L1 may act cooperatively to disrupt CREB phosphorylation. The recent finding that introduction of exogenous UCH-L1 into AD model mice rescues synaptic and memory deficits supports this possibility (Gong *et al.*, 2006).

It should be noted that memory deficits are already evident in young *gad* mice (6 weeks of age). Analysis of AD model mice has shown that the onset of the behavioural phenotype is generally much slower. For example, deficits in visible platform recognition become evident by 9 months of age, and deficits in sensorimotor tasks are clearly manifest by 14 months in the Tg2579 transgenic AD model mice (King & Arendash, 2002). Impairments in passive avoidance and small-pool performance are marked only at 18 and 25 months of age in the APP23 transgenic AD model mice (Kelly *et al.*, 2003). It has not been reported whether UCH-L1 is down-regulated in these model mice. In the APP/PS1 mouse model of AD, on the other hand, relatively young (3- to 4-month-old) mice have impaired contextual learning (Trinchese *et al.*, 2004; Gong *et al.*, 2006), and reduced hippocampal UCH activity is evident at 4–6 months of age (Gong *et al.*, 2006). Whether the onset of the reduction in the hydrolase activity is synchronous with the onset of impaired contextual learning in the APP/PS1 mouse is unknown. This information is necessary to further verify the involvement of UCH-L1 in memory deficits associated with AD and in AD model mice.

Impairment of memory in *gad* mice was associated with impaired transcription-dependent LTP in the hippocampus. Because LTP is a well-known cellular mechanism of memory (reviewed in Bliss & Collingridge, 1993), it is reasonable to speculate that impaired LTP is one of the mechanisms underlying the memory deficits in *gad* mice. Our results provide a possible mechanistic link between the lack of UCH-L1 and impaired LTP: alteration of CREB phosphorylation. Proper timing and persistence of CREB phosphorylation are essential for the gene expression required to maintain LTP in area CA1 of the hippocampus (Impey *et al.*, 1996). After conditioning in the passive avoidance test, cAMP response element-mediated transcription is induced in hippocampal area CA1 (Impey *et al.*, 1998). Thus, the alteration of CREB phosphorylation and subsequent failure to maintain LTP might be responsible for reduced performance of *gad* mice in the passive avoidance test. However, LTP at hippocampal CA1 synapses is dependent on NMDA receptors (Harris *et al.*, 1984; Larson & Lynch, 1988). Phosphorylation of CREB is also NMDA receptor-dependent (Ahmed & Frey, 2005). This type of LTP occurs in various brain regions (reviewed in Martin *et al.*, 2000), and UCH-L1 is expressed in almost all brain regions. Therefore, impaired LTP in other brain regions may also be involved in the poor performance of *gad* mice in the passive avoidance test and other behavioural tests. Postsynaptically, the ubiquitin–proteasome system is involved in activity-dependent changes in postsynaptic protein composition and signalling (Ehlers, 2003; reviewed in Yi & Ehlers, 2007). UCH-L1 has *in vitro* enzymatic activity that exposes the free C-terminus of ubiquitin, which is required for protein ubiquitination (Larsen *et al.*, 1998), and monoubiquitin levels are decreased in *gad* mouse brain (Osaka *et al.*, 2003).

In conclusion, we report that UCH-L1 is required for the maintenance of memory in passive avoidance learning, exploratory behaviour and hippocampal CA1 LTP in mice. We propose that UCH-L1-mediated maintenance of the temporal integrity and persistence of CREB phosphorylation is required for CA1 LTP.

Acknowledgements

We thank Drs Chiaki Itami and Shun Nakamura for their advice in the early stage of this work. We also thank Miss Hisae Kikuchi for her technical assistance. This work was supported in part by Grants-in-Aid for Scientific

Research from the Ministry of Health, Labour and Welfare of Japan, Grants-in-Aid for Scientific Research from the Ministry of Education, Culture, Sports, Science and Technology of Japan, the Program for Promotion of Fundamental Studies in Health Sciences of the National Institute of Biomedical Innovation, and a grant from the Japan Science and Technology Agency.

Abbreviations

Aβ, amyloid β-protein; ACSF, artificial cerebrospinal fluid; AD, Alzheimer's disease; CREB, cyclic AMP response element-binding protein; fEPSPs, field excitatory postsynaptic potentials; *gad*, gracile axonal dystrophy; H&E, hematoxylin and eosin; LTP, long-term potentiation; pCREB, phosphorylated CREB; PD, Parkinson's disease; PKA, protein kinase A; TBS, theta-burst stimulation; UCH-L1, ubiquitin C-terminal hydrolase L1.

References

Abel, T., Nguyen, P.V., Barad, M., Deuel, T.A. & Kandel, E.R. (1997) Genetic demonstration of a role for PKA in the late phase of LTP and in the hippocampus-based long-term memory. *Cell*, **88**, 615–626.

Ahmed, T. & Frey, J.U. (2005) Plasticity-specific phosphorylation of CaMKII, MAP-kinases and CREB during late-LTP in rat hippocampal slices in vitro. *Neuropharmacology*, **49**, 477–492.

Bevilaqua, L., Ardenghi, P., Schroder, N., Bromberg, E., Schmitz, P.K., Schaeffer, E., Quevedo, J., Bianchin, M., Walz, R., Medina, J.H. & Izquierdo, I. (1997) Drugs acting upon the cyclic adenosine monophosphate/protein kinase A signaling pathway modulate memory consolidation when given late after training into rat hippocampus but not amygdala. *Behav. Pharmacol.*, **8**, 331–338.

Bliss, T.V. & Collingridge, G.L. (1993) A synaptic model of memory: long-term potentiation in the hippocampus. *Nature*, **361**, 31–39.

Bouton, M.E., Kenney, F.A. & Rosengard, C. (1990) State-dependent fear extinction with two benzodiazepine tranquilizers. *Behav. Neurosci.*, **104**, 44–55.

Bradshaw, K.D., Emptage, N.L. & Bliss, T.V. (2003) A role for dendritic protein synthesis in hippocampal late LTP. *Eur. J. Neurosci.*, **18**, 3150–3152.

Castegna, A., Aksenov, M., Aksenova, M., Thongboonkerd, V., Klein, J.B., Pierce, W.M., Booze, R., Markesbery, W.M. & Butterfield, D.A. (2002) Proteomic identification of oxidatively modified proteins in Alzheimer's disease brain. Part I: creatine kinase BB, glutamine synthase, and ubiquitin carboxy-terminal hydrolase L-1. *Free Radic. Biol. Med.*, **33**, 562–571.

Chapman, P.F., White, G.L., Jones, M.W., Cooper-Blacketer, D., Marshall, V.J., Irizarry, M., Younkin, L., Good, M.A., Bliss, T.V., Hyman, B.T., Younkin, S.G. & Hsiao, K.K. (1999) Impaired synaptic plasticity and learning in aged amyloid precursor protein transgenic mice. *Nat. Neurosci.*, **2**, 271–276.

Choi, J., Levey, A.I., Weintraub, S.T., Rees, H.D., Gearing, M., Chin, L.S. & Li, L. (2004) Oxidative modifications and down-regulation of ubiquitin carbocyl-terminal hydrolase L1 associated with idiopathic Parkinson's and Alzheimer's diseases. *J. Biol. Chem.*, **279**, 13256–13264.

Ehlers, M.D. (2003) Activity level controls postsynaptic composition and signaling via the ubiquitin-proteasome system. *Nat. Neurosci.*, **6**, 231–242.

Freir, D.B., Holscher, C. & Herron, C.E. (2001) Blockade of long-term potentiation by β-amyloid peptides in the CA1 region of the rat hippocampus in vivo. *J. Neurophysiol.*, **85**, 708–713.

Gong, B., Cao, Z., Zheng, P., Vitolo, O.V., Liu, S., Staniszewski, A., Moolman, D., Zhang, H., Shelanski, M. & Arancio, O. (2006) Ubiquitin hydrolase Uch-L1 rescues beta-amyloid-induced decreases in synaptic function and contextual memory. *Cell*, **126**, 775–788.

Harris, E.W., Ganong, A.H. & Cotman, C.W. (1984) Long-term potentiation in the hippocampus involves activation of N-methyl-D-aspartate receptors. *Brain Res.*, **323**, 132–137.

Hedge, A.N., Inokuchi, K., Pei, W., Casadio, A., Ghirardi, M., Chain, D.G., Martin, K.C., Kandel, E.R. & Schwartz, J.H. (1997) Ubiquitin C-terminal hydrolase is an immediate-early gene essential for long-term facilitation in Aplysia. *Cell*, **89**, 115–126.

Ichihara, N., Wu, J., Chui, D.H., Yamazaki, K., Wakabayashi, T. & Kikuchi, T. (1995) Axonal degeneration promotes abnormal accumulation of amyloid beta-protein in ascending gracile tract of gracile axonal dystrophy (*GAD*) mouse. *Brain Res.*, **695**, 173–178.

Impey, S., Mark, M., Villacres, E.C., Poser, S., Chavkin, C. & Storm, D.R. (1996) Induction of CRE-mediated gene expression by stimuli that generate long-lasting LTP in area CA1 of the hippocampus. *Neuron*, **16**, 973–982.

Impey, S., Smith, D.M., Obrietan, K., Donahue, R., Wade, C. & Storm, D.R. (1998) Stimulation of cAMP response element (CRE)-mediated transcription during contextual learning. *Nat. Neurosci.*, **1**, 595–601.

Kabuta, T., Suzuki, Y. & Wada, K. (2006) Degradation of amyotrophic lateral sclerosis-linked mutant Cu, Zn-superoxide dismutase proteins by macro-autophagy and the proteasome. *J. Biol. Chem.*, **281**, 30524–30533.

Kelly, P.H., Bondolfi, L., Hunziker, D., Schlecht, H.-P., Carver, K., Maguire, E., Arbamowski, D., Wiederhold, K.-H., Sturchler-Pierrat, C., Jucker, M., Bergmann, R., Staufenbiel, M. & Sommer, B. (2003) Progressive age-related impairment of cognitive behavior in APP23 transgenic mice. *Neurobiol. Aging*, **24**, 365–378.

Kikuchi, T., Mukoyama, M., Yamazaki, K. & Moriya, H. (1990) Axonal degeneration of ascending sensory neurons in gracile axonal dystrophy mutant mouse. *Acta Neuropathol.*, **80**, 145–151.

King, D.L. & Arendash, G.W. (2002) Behavioral characterization of the Tg2576 transgenic model of Alzheimer's disease through 19 months. *Physiol. Behav.*, **75**, 627–642.

Larsen, C.N., Krantz, B.A. & Wilkinson, K.D. (1998) Substrate specificity of deubiquitinating enzyme: ubiquitin C-terminal hydrolases. *Biochemistry*, **37**, 3358–3368.

Larson, J. & Lynch, G. (1988) Role of N-methyl-D-aspartate receptors in the induction of synaptic potentiation by burst stimulation patterned after the hippocampal theta-rhythm. *Brain Res.*, **441**, 111–118.

Leroy, E., Boyer, R., Auburger, G., Leube, B., Ulm, G., Mezey, E., Harta, G., Brownstein, M.J., Jonnalagada, S., Chernova, T., Dehejia, A., Lavedan, C., Gasser, T., Steinbach, P.J., Wilkinson, K.D. & Polymeropoulos, M.H. (1998) The ubiquitin pathway in Parkinson's disease. *Nature*, **395**, 451–452.

Lever, C., Burton, S. & O'Keefe, L. (2006) Rearing on hind legs, environmental novelty, and the hippocampal formation. *Rev. Neurosci.*, **17**, 111–133.

Liu, Y.C., Fallon, L., Lashuei, H.A., Liu, Z.H. & Lansbury,P.T. Jr (2002) The UCH-L1 gene encodes two opposing enzymatic activities that affect alpha-synuclein degradation and Parkinson's disease susceptibility. *Cell*, **111**, 209–218.

Malinow, R. & Malenka, R.C. (2002) AMPA receptor trafficking and synaptic plasticity. *Annu. Rev. Neurosci.*, **25**, 103–126.

Maraganore, D.M., Farrer, M.J., Hardly, J.A., Lincoln, S.J., McDonnell, S.K. & Rocca, W.A. (1999) Case-control study of the ubiquitin carboxy-terminal hydrolase L1 gene in Parkinson's disease. *Neurology*, **53**, 1858–1860.

Martin, S.J., Grimwood, P.D. & Morris, R.G.M. (2000) Synaptic plasticity and memory. *Annu. Rev. Neurosci.*, **23**, 649–711.

Morris, R.G., Garrud, P., Rawlins, J.N. & O'Keefe, J. (1982) Place navigation impaired in rats with hippocampal lesions. *Nature*, **297**, 681–683.

Nguyen, P.V., Abel, T. & Kandel, E.R. (1994) Requirement of a critical period of transcription for induction of a late phase of LTP. *Science*, **265**, 1104–1107.

Nguyen, P.V., Duffy, S.N. & Young, J.Z. (2000) Differential maintenance and frequency-dependent tuning of LTP at hippocampal synapses of specific strains of inbred mice. *J. Neurophysiol.*, **84**, 2484–2493.

Nguyen, P.V. & Kandel, E.R. (1997) Brief theta-burst stimulation induces a transcription-dependent late phase of LTP requiring cAMP in area CA1 of the mouse hippocampus. *Learn. Mem.*, **4**, 230–243.

Osaka, H., Wang, Y.-L., Takada, K., Takizawa, S., Setsuie, R., Li, H., Sato, Y., Nishikawa, K., Sun, Y.-J., Sakurai, M., Harada, T., Hara, Y., Kimura, I., Chiba, S., Namikawa, K., Kiyama, H., Noda, M., Aoki, S. & Wada, K. (2003) Ubiquitin carboxy-terminal hydrolase L1 binds to and stabilizes monoubiquitin in neuron. *Human Mol. Genet.*, **12**, 1945–1958.

Saigoh, K., Wang, Y.-L., Suh, J.G., Yamanishi, T., Sakai, Y., Kiyosawa, H., Harada, T., Ichihara, N., Wakana, S., Kikuchi, T. & Wada, K. (1999) Intragenic deletion in the gene encoding ubiquitin carboxy-terminal hydrolase in *gad* mice. *Nat. Genet.*, **23**, 47–51.

Selkoe, D.J. (2002) Alzheimer's disease is a synaptic failure. *Science*, **298**, 789–791.

Shemer, I., Holmgren, C., Min, R., Fulop, L., Zilberter, M., Sousa, K.M., Farkas, T., Hartig, W., Penke, B., Burnashev, N., Tanila, H., Zilberter, Y. & Harkany, T. (2006) Non-fibrillar β-amyloid abates spike-timing-dependent synaptic potentiation at excitatory synapses in layer 2/3 of the neocortex by targeting postsynaptic AMPA receptors. *Eur. J. Neurosci.*, **23**, 2035–2047.

Small, D.H., Mok, S.S. & Bornstein, J.C. (2001) Alzheimer's disease and Aβ toxicity: from top to bottom. *Nat. Rev. Neurosci.*, **2**, 595–598.

Snyder, E.M., Nong, Y., Almeida, C.G., Paul, S., Moran, T., Choi, E.Y., Nairn, A.C., Salter, A.W., Lombroso, P.J., Gouras, G.K. & Greengard, P. (2005) Regulation of NMDA receptor trafficking by amyloid-β. *Nat. Neurosci.*, **8**, 1051–1058.

Takamatsu, I., Sekiguchi, M., Wada, K., Sato, T. & Ozaki, M. (2005) Propofol-mediated impairment of CA1 long-term potentiation in mouse hippocampal slices. *Neurosci. Lett.*, **389**, 129–132.

Trinchese, F., Liu, S., Battaglia, F., Walter, S., Mathews, P.M. & Arancio, O. (2004) Progressive age-related development of Alzheimer-like pathology in APP//PS1 mice. *Ann. Neurol.*, **55**, 801–814.

Vitolo, O.V., Sant'Angelo, A., Costanzo, V., Battaglia, F., Arancio, O. & Shelanski, M. (2002) Amyloid β-peptide inhibition of the PKA/CREB pathway and long-term potentiation: reversibility by drugs that enhance cAMP signaling. *Proc. Natl. Acad. Sci. USA*, **99**, 13217–13221.

Wilkinson, K.D., Lee, K.M., Deshpande, S., Duerksen-Hughes, P., Boss, J.M. & Pohl, J. (1989) The neuron-specific protein PGP 9.5 is a ubiquitin carboxyl-terminal hydrolase. *Science*, **246**, 670–673.

Xue, S. & Jia, J. (2006) Genetic association between ubiquitin carboxy-terminal hydrolase-L1 gene S18Y polymorphism and sporadic Alzheimer's disease in a Chinese Han population. *Brain Res.*, **1087**, 28–32.

Yamada, K., Santo-Yamada, Y. & Wada, K. (2003) Stress-induced impairment of inhibitory avoidance learning in female neuromedin B receptor-deficient mice. *Physiol. Behav.*, **78**, 303–309.

Yamada, K., Santo-Yamada, Y., Wada, E. & Wada, K. (2002) Role of bombesin (BN)-like peptides/receptors in emotional behavior by comparison of three strains of BN-like peptide receptor knockout mice. *Mol. Psychiatry*, **7**, 113–117.

Yao, P.J., Zhu, M., Pyun, E.I., Brooks, A.I., Therianos, S., Meyers, V.E. & Coleman, P.D. (2003) Defects in expression of genes related to synaptic vesicle trafficking in frontal cortex of Alzheimer's disease. *Neurobiol. Dis.*, **12**, 97–109.

Yi, J.J. & Ehlers, M.D. (2007) Emerging roles for ubiquitin and protein degradation in neuronal function. *Pharmacol. Rev.*, **59**, 14–39.

Zushida, K., Sakurai, M., Wada, K. & Sekiguchi, M. (2007) Facilitation of extinction learning for contextual fear memory by PEPA-a potentiator of AMPA receptors. *J. Neurosci.*, **27**, 158–166.

Human Molecular Genetics, 2008, Vol. 17, No. ? *1–15*
doi:10.1093/hmg/ddn037
Advance Access published on xxx

Aberrant molecular properties shared by familial Parkinson's disease-associated mutant UCH-L1 and carbonyl-modified UCH-L1

Tomohiro Kabuta[1,2,*], Rieko Setsuie[1,2], Takeshi Mitsui[1,3], Aiko Kinugawa[1], Mikako Sakurai[1], Shunsuke Aoki[1], Kenko Uchida[3] and Keiji Wada[1,*]

[1]Department of Degenerative Neurological Diseases, National Institute of Neuroscience, National Center of Neurology and Psychiatry, 4-1-1 Ogawahigashi, Kodaira, Tokyo 187-8502, Japan, [2]The Japan Health Sciences Foundation, 13-4 Nihonbashi Kodenma, Chuo-ku, Tokyo 103-0001, Japan and [3]Department of Electrical Engineering and Bioscience, Waseda University, Tokyo 169-8555, Japan

Received January 8, 2008; Revised and Accepted January 30, 2008

Parkinson's disease (PD) is a neurodegenerative disorder characterized by loss of dopaminergic neurons. The I93M mutation in ubiquitin C-terminal hydrolase L1 (UCH-L1) is associated with familial PD, and we have previously shown that the I93M UCH-L1-transgenic mice exhibit dopaminergic cell loss. Over 90% of neurodegenerative diseases, including PD, occur sporadically. However, the molecular mechanisms underlying sporadic PD as well as PD associated with I93M UCH-L1 are largely unknown. UCH-L1 is abundant (1–5% of total soluble protein) in the brain and is a major target of oxidative/carbonyl damage associated with sporadic PD. As well, abnormal microtubule dynamics and tubulin polymerization are associated with several neurodegenerative diseases including frontotemporal dementia and parkinsonism linked to chromosome 17. Here we show that familial PD-associated mutant UCH-L1 and carbonyl-modified UCH-L1 display shared aberrant properties: compared with wild-type UCH-L1, they exhibit increased insolubility and elevated interactions with multiple proteins, which are characteristics of several neurodegenerative diseases-linked mutants. Circular dichroism analyses suggest similar structural changes in both UCH-L1 variants. We further report that one of the proteins interacting with UCH-L1 is tubulin, and that aberrant interaction of mutant or carbonyl-modified UCH-L1 with tubulin modulates tubulin polymerization. These findings may underlie the toxic gain of function by mutant UCH-L1 in familial PD. Our results also suggest that the carbonyl modification of UCH-L1 and subsequent abnormal interactions of carbonyl-modified UCH-L1 with multiple proteins, including tubulin, constitute one of the causes of sporadic PD.

INTRODUCTION

Parkinson's disease (PD) is the most common neurodegenerative movement disorder and is characterized by progressive cell loss confined mostly to dopaminergic neurons in the substantia nigra pars compacta. The I93M mutation in ubiquitin C-terminal hydrolase L1 (UCH-L1) was reported in a German family with dominantly inherited PD (1). To assess the correlation of the I93M mutation and pathogenesis of PD, we have previously generated UCH-L1^{I93M}-transgenic mice. These mice exhibited progressive dopaminergic cell loss in the substantia nigra (2), suggesting that the I93M mutation in UCH-L1 is a causative mutation for PD. The S18Y polymorphism in UCH-L1 has been reported to be associated with decreased risk of PD (3). However, it has also been reported that S18Y is not associated with risk of PD (4).

UCH-L1 is abundant (1–5% of total soluble protein) in the brain (5) and is thought to hydrolyse polymeric ubiquitin and ubiquitin conjugates to monoubiquitin (6). UCH-L1 has also been reported to act as a ubiquitin ligase *in vitro* (7). In

*To whom correspondence should be addressed. Tel: +81 423461715; Fax: +81 423461745; Email: kabuta@ncnp.go.jp; clockkab@ybb.ne.jp (T.K.); wada@ncnp.go.jp (K.W.)

addition to these enzymatic activities, we have found that UCH-L1 binds to and stabilizes monoubiquitin in neurons (8). Our previous studies using circular dichroism (CD) and small-angle neutron scattering strongly suggested that the I93M mutation in UCH-L1 alters the conformation of UCH-L1 (9,10). We have previously shown that mice deficient in UCH-L1 do not exhibit progressive dopaminergic cell loss, in contrast to UCH-L1^{I93M}-transgenic mice (2,8,11), suggesting that a loss or decrease in the level of UCH-L1 is not the main cause of PD, and that UCH-L1^{I93M}-associated PD is caused by an acquired toxicity. Thus, although the hydrolase activity of UCH-L1^{I93M} is decreased (1,9), this decreased activity may not be a major cause of PD.

Increased oxidative stress is associated with neurodegenerative diseases (12,13). In sporadic PD brains, UCH-L1 is a major target of carbonyl formation (12), which is the most widely used marker for oxidative damage to proteins. UCH-L1 has also been identified as a component of several inclusion bodies characteristic of neurodegenerative diseases, including Lewy bodies (14). These findings suggest that UCH-L1 and its modification by carbonyl formation are involved in the cause of sporadic PD. Despite the fact that the majority of PD cases occur sporadically, the molecular mechanisms underlying the causes of sporadic PD, as well as UCH-L1^{I93M}-associated PD, are largely unknown. Moreover, the biochemical properties of UCH-L1^{I93M} and carbonyl-modified UCH-L1 in mammalian cells, such as their protein interactions or detergent insolubility (i.e. the amount of a protein in the insoluble fraction), are poorly understood.

In this study, we analyzed the molecular properties of carbonyl-modified UCH-L1 and UCH-L1^{I93M} and elucidated novel properties of UCH-L1 variants, including protein interactions. We show that carbonyl-modified UCH-L1 and UCH-L1^{I93M} share common properties. Our findings provide novel insights into understanding the mechanisms underlying the toxic gain of function by mutant UCH-L1 and suggest that oxidative stress and subsequent protein interactions of carbonyl-modified UCH-L1 constitute one of the causes of sporadic PD. We also discuss the possible involvement of oxidative modifications of UCH-L1 in other neurodegenerative diseases.

RESULTS

Disease-associated mutants including UCH-L1^{I93M} display aberrant insolubility

Aberrantly increased insolubility compared with wild-type protein is a common biochemical feature of several mutant proteins associated with neurodegenerative diseases: for example, mutant α-synuclein associated with familial PD (15), mutant SOD1 associated with familial amyotrophic lateral sclerosis (ALS) (16,17) and mutant tau associated with frontotemporal dementia and parkinsonism linked to chromosome 17 (18). Although we have previously shown that the insolubility of UCH-L1 in the UCH-L1^{I93M}-transgenic mouse brain is increased compared with that in wild-type mouse (2), the insolubility of UCH-L1^{I93M} itself has been unclear. We observed that pathogenic α-synuclein and SOD1 mutant proteins exhibit increased detergent insolubility in mammalian cells compared with wild-type proteins (Fig. 1A and B). The insolubility of UCH-L1^{I93M} was examined under the same experimental conditions, in which the causative mutants are distinguishable from wild-type proteins. We found that, in dopaminergic SH-SY5Y cells, the protein level of UCH-L1^{I93M} in the insoluble fraction was markedly higher than the levels of UCH-L1^{WT}, UCH-L1^{S18Y}, UCH-L1^{D30K}, which lacks hydrolase activity and binding affinity for ubiquitin (8), and UCH-L1^{C90S}, which lacks hydrolase activity but maintains binding affinity for ubiquitin (8) (Fig. 1C). There was no notable difference among the soluble protein levels (Fig. 1C). The formation of high molecular weight aggregates, which is also a common feature of several mutants, was observed almost exclusively in the insoluble fraction with UCH-L1^{I93M} (Fig. 1C), consistent with the report that UCH-L1^{I93M} produced more aggresomes than UCH-L1^{WT} (19). Increased insolubility of UCH-L1^{I93M} and UCH-L1$^{S18Y/I93M}$ and an increase in the amounts of aggregates specific for these proteins were observed in COS-7 cells (Fig. 1D; Supplementary Material, Fig. S1A), which express very low levels of endogenous UCH-L1. These results demonstrate that UCH-L1^{I93M} shares common features with several mutant proteins linked to neurodegenerative diseases, thus, further supporting the idea that the I93M mutation in UCH-L1 is a causative mutation for PD. Our results also suggest that the insolubility of UCH-L1 is independent of monoubiquitin-binding.

UCH-L1^{I93M} abnormally interacts with multiple proteins

Although increased insolubility is a common characteristic of several mutant proteins associated with neurodegenerative diseases, and this may play a role in the neurotoxicity of the mutant proteins, accumulating evidence suggests that a soluble mutant is the main cause of neurodegeneration (20,21). Studies of dominantly inherited neurodegenerative disease-linked mutants strongly suggest that abnormal physical interactions of the mutant proteins with other proteins constitute a cause of disease (22–26). Hence, we next examined the effect of the I93M mutation on the protein interactions of soluble UCH-L1 using a co-immunoprecipitation (coIP) assay. Silver staining of immunoprecipitant revealed that UCH-L1^{WT} interacts with multiple proteins over 30 kDa (Fig. 1E). We found that the amount of each protein interacting with UCH-L1^{I93M} is mostly higher than the amount interacting with UCH-L1^{WT} or other UCH-L1 variants (Fig. 1F; Supplementary Material, Fig. S1B). Monoubiquitin binding of UCH-L1^{I93M} was decreased compared with that of UCH-L1^{WT} (Fig. 1G), consistent with the decreased hydrolase activity of UCH-L1^{I93M} (1,9). However, the cellular monoubiquitin level in cells expressing UCH-L1^{I93M} was not changed compared with that in cells expressing UCH-L1^{WT} (Fig. 1G). Since UCH-L1^{I93M}-associated PD is presumably caused by an acquired toxicity, the toxic function of UCH-L1^{I93M} may not be mainly mediated by a decreased interaction with monoubiquitin, but rather by aberrantly elevated interactions with multiple other proteins.

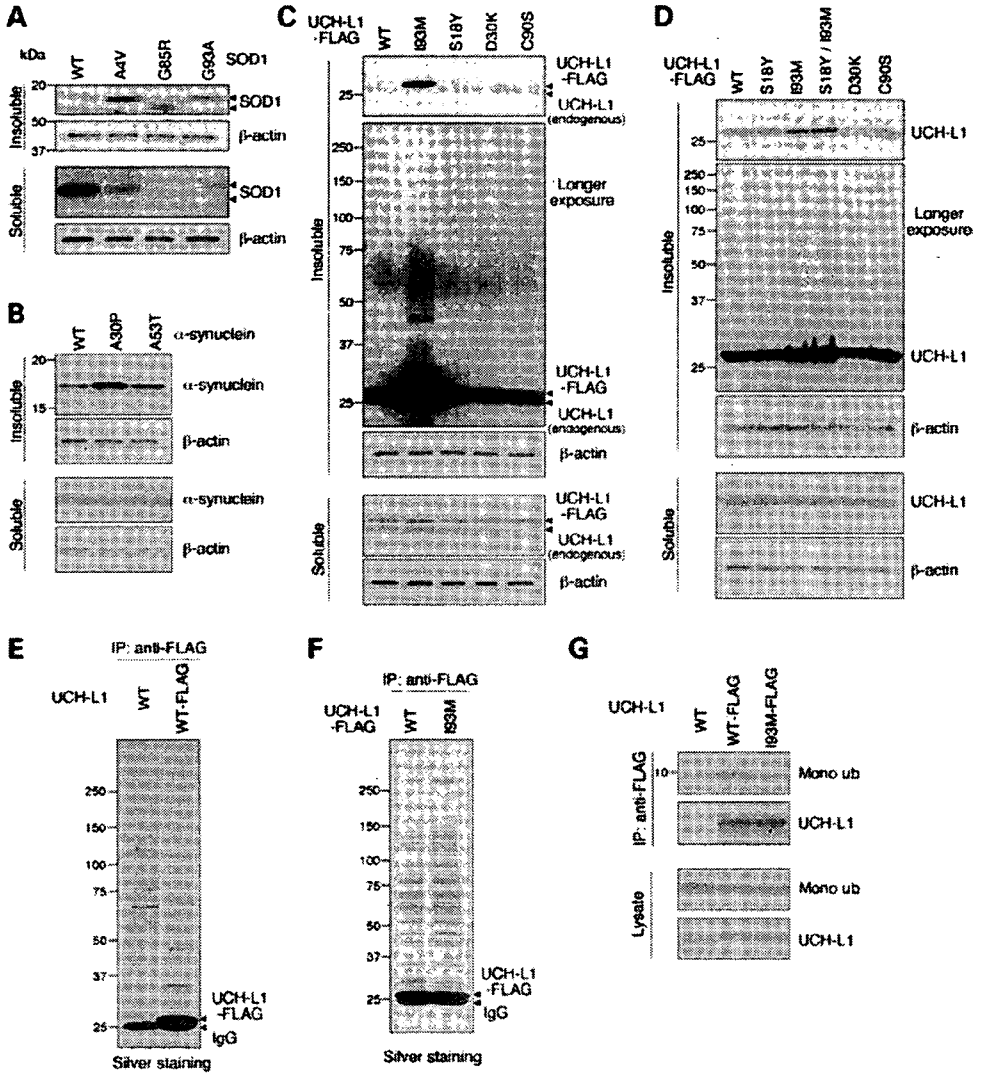

Figure 1. Aberrant biochemical properties of mutant I93M UCH-L1. [(**A**)–(**D**)] SH-SY5Y (A) and (C), Neuro2a (B) and COS-7 cells (D) were transfected with the indicated constructs. Forty-eight hours after transfection, soluble and insoluble fractions were prepared and analyzed by immunoblotting. [(**E**)–(**G**)] COS-7 cells were transfected with the indicated constructs. Cell lysates were immunoprecipitated using anti-FLAG antibody and analyzed by silver staining [(E) and (F)] or by immunoblotting (G). In the presence of FLAG-tagged UCH-L1, UCH-L1-interacting proteins were co-immunoprecipitated with UCH-L1 [(E), lane 2], whereas in the absence of FLAG-tagged UCH-L1, proteins were non-specifically precipitated with anti-FLAG beads [(E), lane 1]. Mono ub, monoubiquitin (G).

Carbonyl-modified UCH-L1 exhibits aberrant properties common to UCH-L1^{I93M}

In the brains of sporadic PD patients, UCH-L1 is a major target of carbonyl formation (12). Carbonyl groups can be introduced into proteins *in vivo* mainly by reactions with 2-alkenals, 4-hydroxy-2-alkenals (HAE) or ketoaldehydes, which are endogenous aldehydic products formed by lipid peroxidation or glycooxidation (27,28). Protein carbonyls can also be produced by metal-catalyzed reactions with H_2O_2 *in vitro* (28,29). To analyze the biochemical properties of carbonyl-modified UCH-L1, we used several carbonyl compounds or H_2O_2 to modify UCH-L1. We have previously reported that UCH-L1 is modified by 4-hydroxy-2-nonenal (HNE) *in vitro* (9). In COS-7 cells transfected with UCH-L1^{WT}, UCH-L1 was modified by physiological concentrations of HNE (10–100 μM) (9) or 4-hydroxy-2-hexenal (HHE) in a dose-dependent manner (Fig. 2A and B; Supplementary Material, Fig. S1C). Carbonyl modification of UCH-L1 was also detected when cells were treated with 100 μM 2-propenal (Fig. 2A), but not with 100 or 500 μM methylglyoxal, 100 or 500 μM malondialdehyde, both of which are ketoaldehydes, or 0.1 or 1 mM H_2O_2 (data not shown). Thus, carbonyl-modified UCH-L1 can be produced by reactions with HAE or 2-alkenals in mammalian cells.

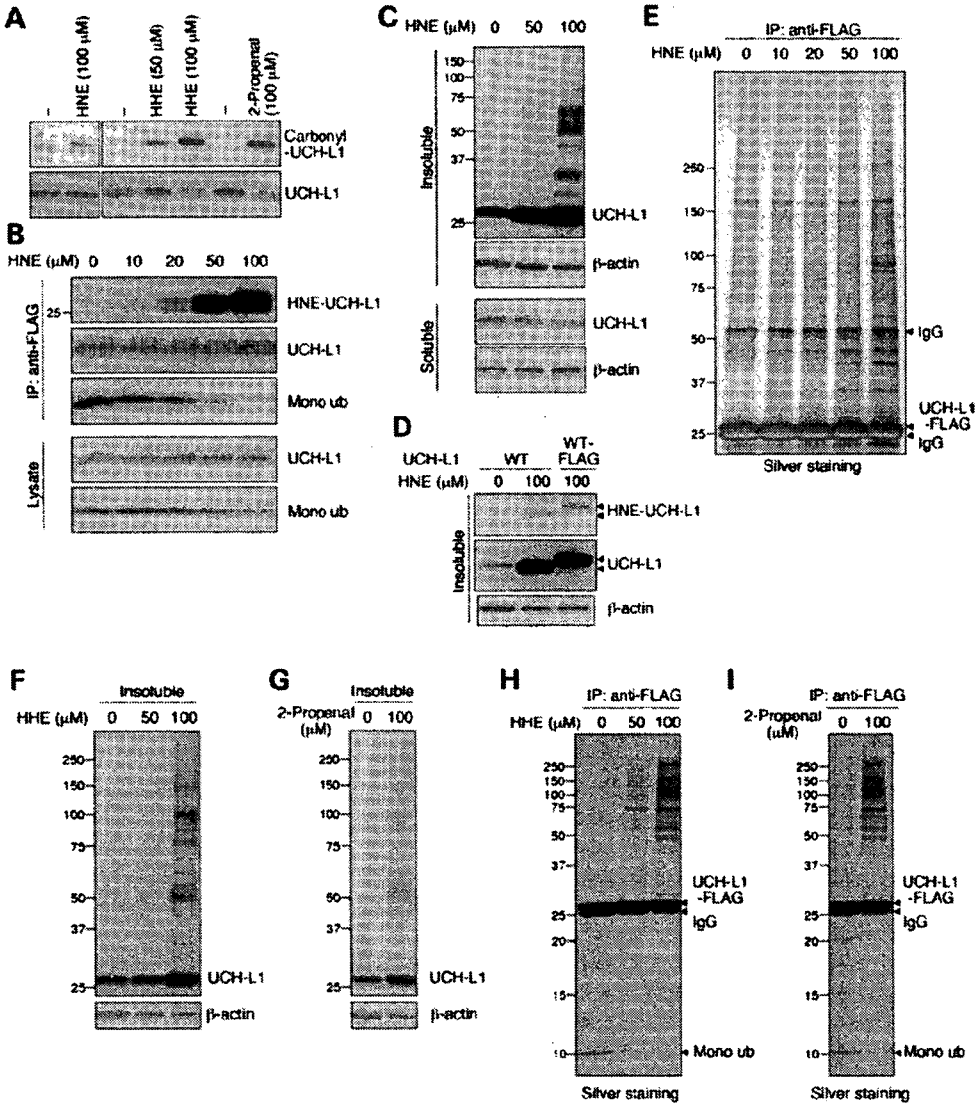

Figure 2. Abnormal biochemical properties of carbonyl-modified UCH-L1. **(A)** COS-7 cells transfected with FLAG-tagged UCH-L1^{WT} were treated with or without the indicated concentrations of carbonyl compounds for 90 min, and immunoprecipitation was performed using anti-FLAG antibody. To detect carbonyl-modified UCH-L1, immunoprecipitants were derivatized with DNPH and immunoblotted using anti-DNP or anti-UCH-L1 antibodies. **[(B), (E), (H) and (I)]** COS-7 cells transfected with FLAG-tagged UCH-L1^{WT} were treated with the indicated concentrations of HNE [(B) and (E)], HHE (H) or 2-propenal (I) for 90 min, and immunoprecipitation was performed using anti-FLAG antibody. Immunoprecipitants were analyzed by immunoblotting or by silver staining. **[(C), (F) and (G)]** COS-7 cells transfected with FLAG-tagged UCH-L1^{WT} were treated with the indicated concentrations of HNE (C), HHE (F) or 2-propenal (G). Soluble and insoluble fractions were analyzed by immunoblotting. **(D)** COS-7 cells transfected with the indicated constructs were treated with or without HNE, and insoluble fractions were prepared. Immunoblotting shows that the insoluble UCH-L1 that is accumulated upon HNE treatment is modified by HNE.

Interestingly, carbonyl-modified UCH-L1 and UCH-L1^{I93M} exhibit common biochemical properties: ubiquitin binding of HNE-modified UCH-L1 was decreased (Fig. 2B), and both the insolubility of HNE-modified UCH-L1 and the interactions of HNE-modified UCH-L1 with proteins over 30 kDa were increased, compared with those of UCH-L1^{WT} (Fig. 2C–E). HHE and 2-propenal had similar effects to HNE (Fig. 2F–I). Treatment of cells with 100 μM H_2O_2, methylglyoxal or malondialdehyde had no effect on the insolubility of UCH-L1 or the interactions of UCH-L1 with other proteins (data not shown). Consistent with the report that UCH-L1 is a major target of carbonyl formation in the brains of sporadic PD patients (12), UCH-L1 is a major target of carbonyl modification in cells treated with HNE (Fig. 3A). We used the EF1 promoter to yield abundant expression of UCH-L1 in this experiment, since the amount of UCH-L1 is 1–5% of

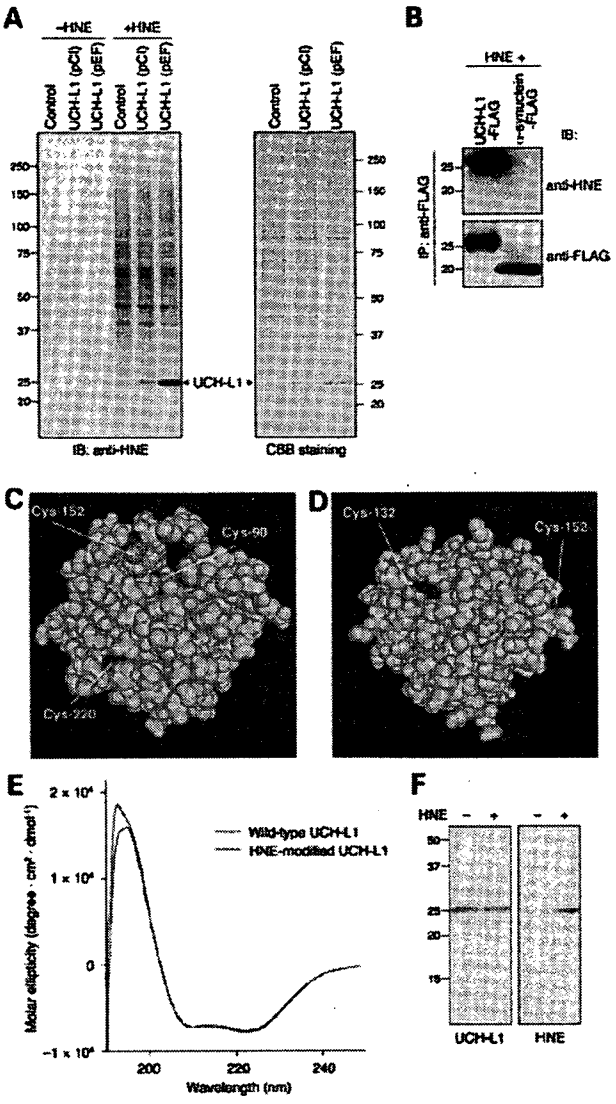

Figure 3. Susceptibility of UCH-L1 to HNE modification and structural properties of UCH-L1 variants. (**A**) COS-7 cells transfected with the indicated constructs were treated with or without 100 μM HNE and analyzed by immunoblotting and CBB staining. (**B**) COS-7 cells transfected with the indicated constructs were treated with 100 μM of HNE, and immunoprecipitation was performed using anti-FLAG antibody. Immunoprecipitants were analyzed by immunoblotting. [(**C**) and (**D**)] Structural model for human UCH-L1. Cys-90, Cys-152 and Cys-220 sidechains are shown in magenta, and backbones are shown in blue (C), using Cn3D software (version 4.1) and NCBI's structural model (mmdbId:38174). Cys-132 and Cys-152 sidechains are shown in magenta, and backbones are shown in blue (D). (**E**) CD spectra (mean residue ellipticity) for recombinant human UCH-L1 proteins. Wild-type UCH-L1 is shown in red and HNE-modified UCH-L1 in blue. (**F**) HNE modification of the recombinant UCH-L1 used in (E) was analyzed by immunoblotting. Modification of UCH-L1 by HNE was detected.

soluble protein in the brain (5). These results suggest that the carbonyl-modified UCH-L1 in sporadic PD brains functions as a causative factor for disease in a similar manner to UCH-L1^{I93M}.

Cys-90 and Cys-152 of UCH-L1 are targets for HAE modification

The appearance of HNE-modified proteins in nigral neurons has been shown to be associated with sporadic PD (30,31). Therefore, we next determined the HNE-modified amino acid residues of UCH-L1 that regulate its insolubility and protein interactions. HNE can form covalent cross-links with cysteine, lysine and histidine residues in proteins (28). To test the specificity of HNE modification in mammalian cells, we used cells transfected with α-synuclein, which contains no cysteine residues. HNE modification of α-synuclein was not detected when cells were treated with 100 μM HNE (Fig. 3B). These results suggest that among the amino acid residues of UCH-L1, cysteine residues are the primary target for HAE. We speculated that Cys-90 is accessible to HAE, since it is a ubiquitin-binding residue. Using the three-dimensional structure of human UCH-L1 (32), we observed that not only Cys-90 but also Cys-132 and Cys-152 are located on the surface of the protein (Fig. 3C and D). Thus, we tested the insolubility and protein interactions using C90S, C132S and C152S UCH-L1 mutant proteins. We also used C220S UCH-L1 as a control. We found that the C152S mutant bound to monoubiquitin in both HNE-treated cells and untreated cells (Fig. 4A). UCH-L1^{C90S} did not exhibit notably increased insolubility upon HNE-treatment compared with UCH-L1^{WT} (1.3-fold increase in UCH-L1^{C90S}, 2.5-fold increase in UCH-L1^{WT}) (Fig. 4B). The amount of proteins over 30 kDa interacting with UCH-L1^{C90S} was markedly lower than that interacting with UCH-L1^{WT} when cells were treated with HNE (Fig. 4C). Similar results were obtained when cells were treated with HHE (Fig. 4E and F; Supplementary Material, Fig. S1D). Mutations at Cys-132 and Cys-220 had no effect on protein insolubility or interactions (Fig. 4A–C). Consistent with these results, HNE modification of C90S and C152S mutants was decreased compared with that of UCH-L1^{WT} when cells were treated with HNE (~40 and 60% decrease, respectively) (Fig. 4D). These results indicate that HAE modification of UCH-L1 at Cys-90 increases the insolubility and interactions of UCH-L1, and modification of Cys-152 reduces monoubiquitin binding. The level of HNE modification of UCH-L1^{I93M} upon HNE-treatment was markedly lower than that of UCH-L1^{WT} (Fig. 4G). Since the location of Cys-90 is close to Ile-93 (Supplementary Material, Fig. S2), it is possible that the I93M mutation and HAE modification at Cys-90 cause similar structural changes in UCH-L1.

HNE modification causes structural changes in UCH-L1

To address the structural changes in carbonyl-modified UCH-L1, we used CD spectroscopy to estimate the secondary structure. We have previously shown that, compared with UCH-L1^{WT}, the I93M mutant displays lower ellipticity around 195 nm, suggesting a decreased α-helix content, and an increase in the content of β-sheet (9,10). Relative to wild-type protein, HNE-modified UCH-L1 also displayed a lower peak around 190–195 nm (Fig. 3E and F). The relative proportions of α-helix, β-sheet and other secondary structural features in these proteins were estimated from mean residue ellipticity data. HNE-modified UCH-L1 also exhibited

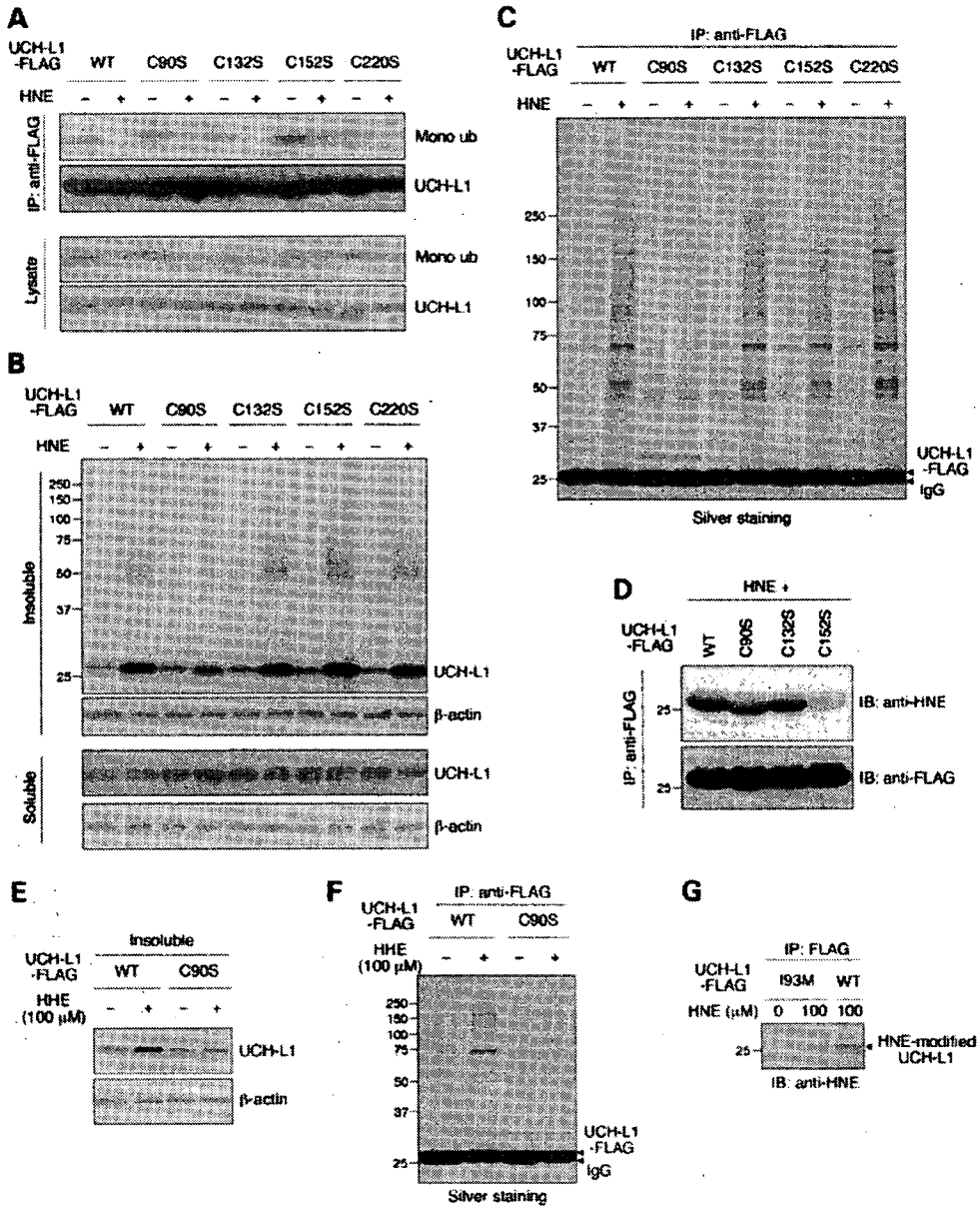

Figure 4. Cysteine residues of UCH-L1 modified by HAE. [(**A**), (**C**), (**D**), (**F**) and (**G**)] COS-7 cells transfected with the indicated constructs were treated with or without 100 μM HNE or HHE. Immunoprecipitation was performed using anti-FLAG antibody, and immunoprecipitants were analyzed by immunoblotting or by silver staining. [(**B**) and (**E**)] COS-7 cells transfected with the indicated constructs were treated with or without 100 μM HNE or HHE. Soluble and insoluble fractions were analyzed by immunoblotting.

decreased α-helix content, and an increase in the content of β-sheet compared with UCH-L1^{WT} (42.9% α-helix, 20.9% β-sheet, 20.6% β-turn and 15.7% random for UCH-L1^{WT}, and 34.0% α-helix, 27.3% β-sheet, 22.3% β-turn and 16.4% random for HNE-modified UCH-L1). These results suggest that UCH-L1^{I93M} and carbonyl-modified UCH-L1 adopt a similar aberrant structure.

The ALS-linked mutation in SOD1 increases its hydrophobicity, which may promote aberrant interactions of SOD1 with other cellular constituents (33). However, the interactions of UCH-L1^{I93M} or HNE-modified UCH-L1 with hydrophobic beads were not altered relative to those of UCH-L1^{WT} (data not shown), indicating that the I93M mutation and HNE modification of UCH-L1 do not increase its hydrophobicity. Considering the fact that unnatural β-sheet proteins readily become insoluble or form further β-hydrogen-bonding with other β-strands they encounter (34), our results suggest that the increased insolubility and protein interactions of abnormal UCH-L1 are due to the increased β-sheet content of UCH-L1.

UCH-L1 physically interacts with tubulin

To understand the molecular mechanism underlying toxic gain of function by UCH-L1, we attempted to identify UCH-L1^{I93M}-interacting proteins by coIP assay and subsequent LC-MS/MS analysis (Fig. 5A). A database search of the peptide sequences obtained identified α-tubulin as a UCH-L1^{I93M}-interacting protein (Supplementary Material, Table S1). The interaction between UCH-L1 and endogenous α-tubulin was confirmed with transiently expressed UCH-L1 (Fig. 5B and C). The interaction of UCH-L1^{I93M} with α-tubulin was increased compared with that of UCH-L1^{WT} (Fig. 5B). We detected the interaction of endogenous α-tubulin with endogenous UCH-L1 using Neuro2a cells (Fig. 5D). Tubulin is composed of a heterodimer of α- and β-tubulin, and we confirmed, using native-PAGE, that tubulin exists as a heterodimer in cell lysates in coIP experimental conditions (data not shown), indicating that UCH-L1 interacts with tubulin. Indeed, β-tubulin was also precipitated with UCH-L1 (Supplementary Material, Fig. S3). In contrast to tubulin, interaction of β-actin with UCH-L1 was not detected (Fig. 5C). To test whether UCH-L1 directly interacts with tubulin, we performed pull-down assay using recombinant UCH-L1 and purified tubulin. Direct interaction of UCH-L1 with tubulin was observed (Fig. 5E).

Since the interactions between UCH-L1 and proteins over 30 kDa are increased by carbonyl modification or I93M mutation of UCH-L1, we tested the effects of HAE on the interaction of UCH-L1 with tubulin. We found that HAE modification of UCH-L1 promotes interactions between UCH-L1 and tubulin (Fig. 5F, G and I). In addition, a coIP assay using C90S, C132S and C152S UCH-L1 mutants showed less binding of UCH-L1^{C90S} to tubulin than UCH-L1^{WT} did, when cells were treated with HNE or HHE (Fig. 5G–I), indicating that the increased interaction of UCH-L1 with tubulin is caused by the HAE modification of Cys-90 of UCH-L1. These results are consistent with the results showing that the HAE modification of Cys-90 of UCH-L1 promotes the interaction of UCH-L1 with multiple proteins. The I93M mutation and HNE modification of UCH-L1 also promote direct interactions between UCH-L1 and tubulin (data not shown). Thus, UCH-L1^{I93M} and HNE-UCH-L1 also exhibit common biochemical properties with respect to the interactions with tubulin.

Both UCH-L1^{I93M} and carbonyl-modified UCH-L1 aberrantly promote tubulin polymerization

Microtubules are dynamic polymers composed of tubulin that continuously grow and shorten through tubulin addition and loss at the microtubule ends. Microtubule-stabilizing agents such as paclitaxel, which promote tubulin polymerization and suppress microtubule dynamics, are effective chemotherapeutic agents for the treatment of many cancers. However, neuropathy is a major adverse effect of microtubule-stabilizing agents-based chemotherapy (35). Paclitaxel induces apoptosis in cortical neurons by a mechanism independent of its cell cycle effects, because postnatal cortical neurons are postmitotic (36). These findings indicate that tubulin polymerization must be tightly regulated for neurons to function and remain viable. Furthermore, abnormal microtubule dynamics and tubulin polymerization are associated with several neurodegenerative diseases including frontotemporal dementia and parkinsonism linked to chromosome 17 (37,38). Therefore, we examined the effects of UCH-L1^{WT}, UCH-L1^{I93M} and HNE-UCH-L1 on tubulin polymerization using an *in vitro* assay. Interestingly, both UCH-L1^{I93M} and HNE-UCH-L1 promote tubulin polymerization, although UCH-L1^{WT} had almost no effect on it (Fig. 6A and B). Promotion of tubulin polymerization may result in a stabilization of microtubules because of the dynamic instability of microtubules. To test whether abnormal UCH-L1 also promotes tubulin polymerization in mammalian cells, we analyzed the amounts of soluble, polymeric and total tubulin in cells expressing UCH-L1^{I93M}. Although transient expression of UCH-L1^{I93M} had no effect on the amount of total tubulin (Fig. 5B), cells stably expressing UCH-L1^{I93M} contained increased amount of total tubulin compared with control cells or cells expressing other UCH-L1 variants (Fig. 6C). Consistent with the *in vitro* polymerization assay, the amount of polymeric tubulin was increased in cells expressing UCH-L1^{I93M}, whereas the amount of soluble tubulin was not (~1.4 and 1.0-fold increase, respectively, compared with the amount of tubulin in cells expressing UCH-L1^{WT}) (Fig. 6D). The amount of β-actin was not affected by the expression of UCH-L1 variants (Fig. 6C and D), also consistent with the results showing that UCH-L1 does not interact with β-actin. We did not detect specific interaction of UCH-L1 with polymerized tubulin (Fig. 6E), indicating that UCH-L1 may not interact with microtubules, although the possibility is not excluded that they can interact under certain conditions or at a limited number of sites such as the microtubule ends.

Since D30K and C90S mutations had no effect on the interaction of UCH-L1 and tubulin (Fig. 5B), we speculated that the tubulin-binding region of UCH-L1 is different from ubiquitin-binding region. To elucidate the amino acid residues of UCH-L1 involved in the interaction with tubulin and to show that modulation of tubulin polymerization is caused by the increased interaction of UCH-L1 with tubulin, we made a series of alanine substitutions of basic and acidic residues located on the surface of UCH-L1 and performed coIP assays using these mutants (Fig. 7A; Supplementary Material, Fig. S3). The R63A and H185A mutants displayed increased interactions with tubulin (Fig. 7A), indicating that Arg-63 and His-185, which are distinct from the ubiquitin-binding region (Fig. 7B), are involved in this interaction. The increased interactions of R63A and H185A UCH-L1 with tubulin may be caused by altered ionic interactions. In contrast to the I93M mutant or HNE-UCH-L1, the R63A mutant caused a decrease in tubulin polymerization (Fig. 7C). Although UCH-L1^{R63A} has opposite effects to the I93M mutant or HNE-UCH-L1, it also modulated tubulin polymerization. Thus, modulation of tubulin polymerization by UCH-L1 variants is caused by the abnormally increased interaction of UCH-L1 with tubulin.

From our results, we hypothesized that UCH-L1^{I93M}-associated neurodegeneration or PD is at least partly mediated by aberrant tubulin polymerization. Therefore, we tested the effects of UCH-L1^{I93M} and paclitaxel on neuronal cell death using differentiated Neuro2a cells, which

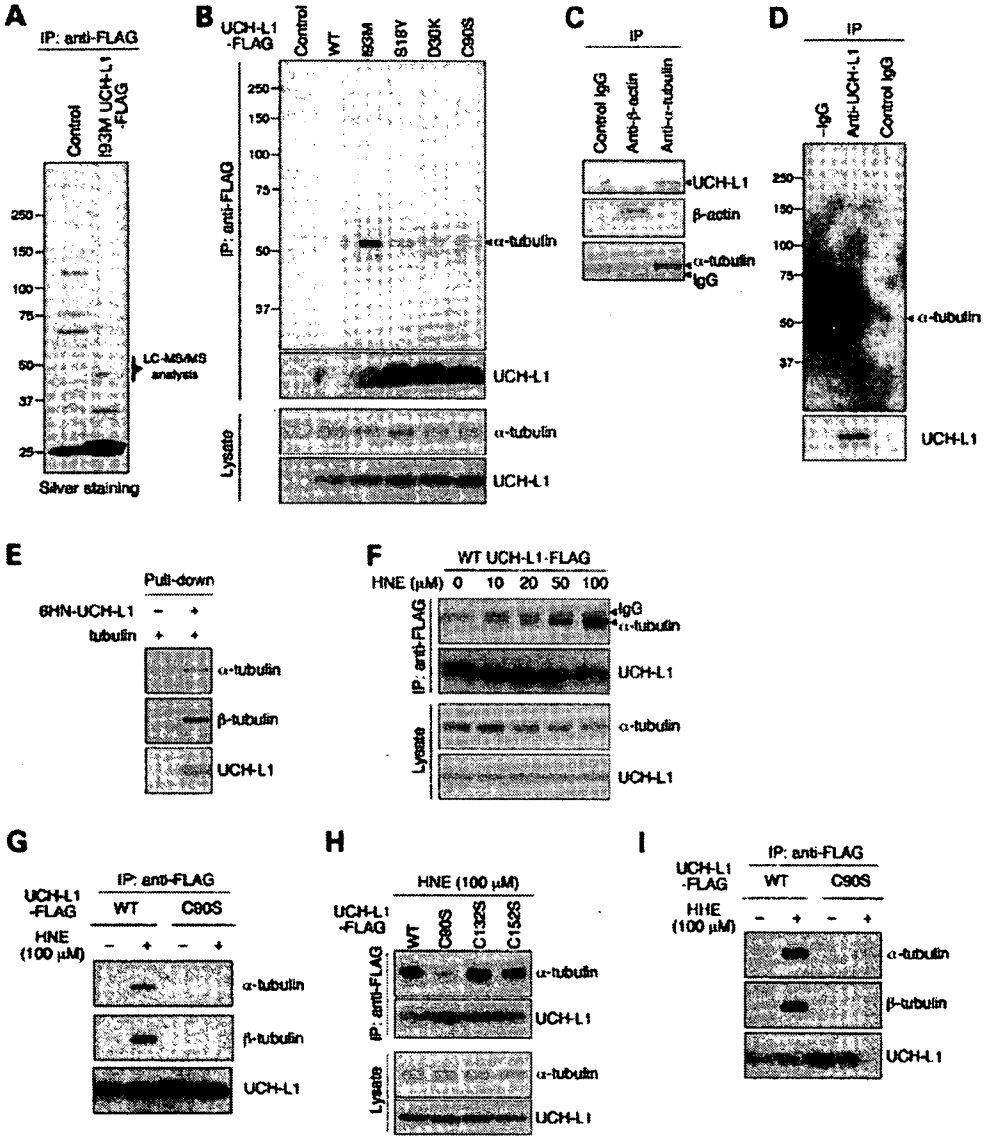

Figure 5. Physical interactions of UCH-L1 with tubulin. (**A**) Lysates of HeLa cells transfected with the indicated constructs (control: GFP) were immunoprecipitated with anti-FLAG antibody and analyzed by silver staining. Proteins ~50 kDa in size were subjected to LC-MS/MS analysis. (**B**) Lysates of COS-7 cells transfected with the indicated constructs (control: empty vector) were immunoprecipitated with anti-FLAG antibody and analyzed by immunoblotting. (**C**) Lysates of NIH-3T3 cells stably expressing FLAG-HA-tagged UCH-L1 were immunoprecipitated with the indicated antibodies and analyzed by immunoblotting. (**D**) Lysates of Neuro2a cells were immunoprecipitated with control IgG or anti-UCH-L1 antibody and analyzed by immunoblotting. -IgG, without IgG. (**E**) A pull-down assay was performed using the indicated purified proteins. [(**F**)–(**I**)] COS-7 cells transfected with the indicated constructs were treated with the indicated concentrations of HNE. Lysates were immunoprecipitated with anti-FLAG antibody and analyzed by immunoblotting.

have been used to assess the toxicity of mutant proteins linked to neurodegenerative diseases (17,39,40). We confirmed that paclitaxel does not interfere with the interaction between UCH-L1 and tubulin (data not shown). Treatment of cells with 5 μM paclitaxel slightly but significantly elevated cell death in cells expressing UCH-L1^{I93M}, but had no effect in cells expressing UCH-L1^{WT} (Fig. 6F). This indicated that the toxicity of UCH-L1^{I93M} may be at least in part mediated by aberrant microtubule dynamics or tubulin polymerization. Given that tightly regulated tubulin polymerization is necessary for neurons to be viable, our findings strongly suggest that aberrant tubulin polymerization caused by UCH-L1^{I93M} underlies the toxic gain of function of mutant UCH-L1, and that carbonyl-modified UCH-L1 also functions as a toxic protein in neurons. We propose that interactions of mutant or carbonyl-modified UCH-L1 with other proteins, including tubulin, constitute one of the causes of not only familial PD, but also sporadic PD (Fig. 7D).